



**Politecnico
di Torino**

POLITECNICO DI TORINO

**DIPARTIMENTO DI INGEGNERIA MECCANICA E
AEROSPAZIALE**

**Master's Degree in Biomedical Engineering
A.Y. 2021-2022**

**Design of nano-formulations to transport
anti-cancer drugs**

Supervisors:

**Prof. Ciardelli Gianluca
Prof. Tuszynski Jacek Adam
Prof. Mattu Clara**

Candidate:

Gaglio Cesare Gabriele

Abstract

Microtubules-targeting agents (MTAs) are an attractive class of compounds that has been broadly used in cancer treatment since the 1960s. Their main mechanism of action is based on their interaction with microtubules, one of the principal components of the cell cytoskeleton, blocking cell division at the mitotic phase and inducing apoptosis. Microtubules are formed by tubulin, which is a heterodimer composed of α - and β -tubulin. MTAs usually bind to β -tubulin and can be divided into microtubules stabilizing or destabilizing agents, either inducing tubulin polymerization or depolymerization, respectively. MTAs can also act as anti-angiogenic agents or vascular-disruptive agents (VDAs). Three main families of MTAs are known, the taxanes, the vinca alkaloids and colchicine and its derivatives, the most used being the first two groups, although every year new classes of compounds and specific binding sites are being discovered. The main issues with the use of MTAs are their scarce selectivity, as microtubules are present in cells independently of them being cancerous or normal ones, and the multi-drug resistance of cancer cells, that be also acquired after long-time treatment with MTAs. The ideal MTA should selectively attack cancer cells and elude multi-drug resistance mechanisms. Selectivity can be achieved by targeting tubulin isotypes that are overexpressed in tumor tissues and underexpressed in healthy tissues, multi-drug resistance can be eluded by avoiding interaction between the drug and the main transmembrane efflux pumps such as P-gp, one of the most studied proteins of the ATP-binding cassette family that contributes to multi-drug resistance, and by regulating the tubulin isotype expression in cancer cells. Colchicine is an alkaloid compound that received FDA approval for the treatment of the symptoms of gout and Familial Mediterranean Fever in 2009 . However, other off-label uses have been reported and its use as anti-cancer compound has been investigated. Colchicine is an interesting compound in cancer treatment as, unlike taxanes and vinca alkaloids, is capable of eluding one mechanism of resistance in cancer cells; indeed, its efficacy is not reduced by the overexpression of β III-tubulin that is commonly found in cancer cells. Unfortunately, the use of colchicine is hindered by its high toxicity and poor bioavailability. Colchicine presents high toxicity and a narrow therapeutic window, which means that the range between the therapeutic and the toxic dosage is small, and occasionally the two dosages overlap. When administered orally, colchicine has been associated with gastrointestinal side effects in most patients, while intravenous administration can cause more severe side effects, such as tissue necrosis, intravascular coagulation and even death. For

this reason, the latter administration route has been banned in 2008 by FDA. To overcome the limitations imposed by the high toxicity and poor solubility of the compound, several colchicine-derivatives have been proposed. Among these, CCI-001, a novel colchicine derivative, developed, synthesized and patented by Professor Tuszynski et al. in the Department of Oncology, University of Alberta, Edmonton, Canada, has demonstrated promising results in cancer treatment. CCI-001 presents a greater affinity for β -III tubulin rather than β -IV tubulin like colchicine. β -III tubulin is overexpressed in many tumors and silenced in healthy cells, so targeting this isotype can help drug selectivity toward cancer cells, reducing drug toxicity. CCI-001 outperformed other state of the art drugs that are currently marketed in *in vitro* studies and showed promising results in *in vivo* studies. Moreover, a clinical trial on CCI-001, intended for patient with recurring or metastatic solid tumors, is currently ongoing.

Unfortunately, CCI-001 is highly hydrophobic, resulting in a low absorption rate and in difficult administration. Therefore, new delivery systems are needed to improve the biodistribution of this drug while maintaining its high efficacy against cancer cells. In this work, an effective nanoformulation of CCI-001, based on shell-core pegylated nanoparticles (NPs), with a polymeric core and a lipidic shell, was produced. The NPs are obtained by the solvent displacement method, also called nanoprecipitation. Different core polymers, PLGA and NHSC2000, a proprietary polyurethane, were used and modifications of the traditional protocol were tested in order to improve drug entrapment efficacy. Yield, particle size, zeta potential, morphology and drug entrapment efficacy were first assessed, showing that nanoparticles possess a small size, a narrow size distribution and stability in aqueous solution at 4°C for up to a week. NHSC2000 was ultimately chosen as polymer, with an average EE% of 6%, much higher compared with the results achieved with PLGA (average EE% of 1%). Finally, *in vitro* studies on U87MG cells were performed. Cytotoxicity was assessed both on 2D and 3D (spheroids) cultures, comparing the efficacy of free CCI-001 and loaded nanoparticles. Furthermore, cell internalization studies were performed. *In vitro* studies on U87 and Mia-PaCa-2 cells demonstrated good cytotoxicity of drug-loaded NPs, while empty carriers did not significantly affect cell viability. Overall, our results showed that nanoformulations of CCI-001 can be obtained with high loading efficacy without altering the anti-cancer effect of the drug, warranting their further investigation.

Table of Contents

List of Figures	iv
List of Tables	vi
1 Introduction	1
1.1 Clinical Rationale: Cancer	1
1.1.1 Traditional therapies in cancer treatment	2
1.1.2 Application of nanomedicines in cancer treatment.	3
1.2 Microtubules	5
1.2.1 Microtubules Dynamics	6
1.2.2 Tubulin isotypes	7
1.3 Microtubules-Targeting Agents	10
1.3.1 MTAs effects on cancer cells	11
1.3.2 MTAs effects on tumoral vasculature	12
1.3.3 Multi-Drug Resistance in MTAs	13
1.4 Colchicine	13
1.4.1 Colchicine mechanism of action	14
1.4.2 Colchicine derivatives: CCI-001	15
1.5 CCI-001 Nanoformulations	17
1.6 Nanoprecipitation	17
1.7 Aim of the work	19
2 Materials and methods	20
2.1 Materials	20
2.2 Instruments	20
2.3 NPs synthesis	21
2.3.1 Nanoprecipitation	21
2.3.2 Nanoprecipitation - Modified Protocol	21
2.4 Characterization Methods	23
2.4.1 Size and Zeta Potential	23
2.4.2 Drug Entrapment Efficacy and Drug Release	24
2.4.3 Yield	25
2.4.4 Morphology	25
2.5 In Vitro Studies	25

2.5.1	Cell culture	26
2.5.2	Spheroid culture	26
2.5.3	Citotoxicity evaluation	26
2.5.4	Internalization and infiltration evaluation	27
3	Results and discussion	28
3.1	Nanoparticles Characterization	28
3.1.1	Size, PDI and Zeta Potential	28
3.1.2	Drug Entrapment Efficiency	30
3.1.3	Drug Release Test	31
3.1.4	Yield	31
3.1.5	Stability in aqueous solution	32
3.1.6	Morphology	33
3.2	In vitro studies	34
3.2.1	Mia-PaCa-2 2D Culture	34
3.2.2	U87MG 2D Culture	36
3.2.3	Nanoparticles' U87MG cells internalization	38
3.2.4	U87MG Spheroids	39
3.2.5	Nanoparticles' U87MG spheroids infiltration	41
4	Conclusions	42
5	Acknowledgements	43
	References	44

List of Figures

1	Schematic representation of passive and active targeting [16].	3
2	Microtubule structure. From THE CELL, Fourth Edition, Figure 12.42.	6
3	Dynamic instability representation, growth (rescue) and depolymerization (catastrophe) cycles are highlighted [34].	7
4	Overview on the strategies to overcome β III-tubulin overexpression, [37].	9
5	MTAs binding sites on α -tubulin β -tubulin heterodimer. α -tubulin is represented on the left, β -tubulin is represented on the right, [51].	11

6	Schematic representation of VDAs and anti-angiogenic drugs mechanisms, [63].	12
7	Colchicine chemical structure.	13
8	CCI-001 chemical structure.	15
9	Schematic illustration of the nanoprecipitation, or solvent displacement method.	18
10	Nanoprecipitation protocol; Step 1 and 2 are added for the modified protocol. Illustration created with BioRender.com.	22
11	Calibration curve for HPLC, curve equation and R^2 value are shown.	25
12	a) Size, b) PDI and size distribution c),d),e), and f) comparison between NSHC2000 and PLGA blank/loaded nanoparticles.	28
13	Zeta Potential comparison between NSHC2000 and PLGA blank/loaded nanoparticles.	29
14	a) Size and b) PDI comparison between NSHC2000 and PLGA nanoparticles obtained with different protocols.	29
15	Zeta potential comparison between NSHC2000 and PLGA nanoparticles obtained with different protocols.	29
16	Drug Entrapment Efficacy comparison between original and modified protocol for both a) NSHC2000 and b) PLGA.	30
17	CCI-001 cumulative release in ddH ₂ O at 37°C over a week.	31
18	Process yield for NSHC2000 loaded NPs.	31
19	Size and Zeta Potential measurements over a week. NPs were stored in ddH ₂ O at 4°C.	32
20	SEM images of blank a), c) and NSHC2000-loaded nanoparticles b),d), at different magnifications.	33
21	Comparison between MiaPaCa-2 cells viabilities resulting from treatments with free CCI-001 and CCI-001-loaded NPs at 1 nM, 5 nM, 10 nM, 20 nM, 50 nM and 100 nM at 24h, 48h, 72h.	34
22	Cells images of MiaPaCa-2 cells treated with a) free CCI-001 and b) CCI-001-loaded NPs at 1 nM, 5 nM, 10 nM, 20 nM, 50 nM and 100 nM at 24h, 48h, 72h. Untreated cells are reported as control group. Scale bar=200 μ m	35
23	Comparison between U87MG cells viabilities resulting from treatments with free CCI-001 and CCI-001-loaded NPs at 1 nM, 5 nM, 10 nM, 20 nM, 50 nM and 100 nM at 24h, 48h, 72h.	36

24	Cells images of U87MG cells treated with a) free CCI-001 and b) CCI-001-loaded NPs at 1 nM, 5 nM, 10 nM, 20 nM, 50 nM and 100 nM at 24h, 48h, 72h. Untreated cells are reported as control group. Scale bar=200 μm	37
25	RGB images of U87MG GFP treated with Rhod-NPs at three concentrations (100nM, 1 μM and 10 μM) Scale bar=100 μm	38
26	Comparison between U87MG spheroids viabilities resulting from treatments with free CCI-001 and CCI-001-loaded NPs at 1 nM, 5 nM, 10 nM, 20 nM, 50 nM and 100 nM at 24h, 48h, 72h.	39
27	Cells images of MiaPaCa-2 cells treated with a) free CCI-001 and b) CCI-001-loaded NPs at 1 nM, 5 nM, 10 nM, 20 nM, 50 nM and 100 nM at 24h, 48h, 72h. Untreated cells are reported as control group. Scale bar=200 μm	40
28	RGB images of U87MG GFP spheroids, treated with two Rhod-NPs concentrations (50 nM, 100 nM) and observed at 48h and 72h. a), b), c), and d) are superimposed images, e), f), g), h) show both frontal and lateral projections of the single slices for a given point, indicated by a yellow scope. Scale bar=250 μm	41

List of Tables

1	List of instruments used.	20
2	Samples used to plot the calibration curve	24

1 Introduction

1.1 Clinical Rationale: Cancer

Cancer is the second leading cause of death globally [1]. In 2020, cancer was responsible for nearly 10 million deaths representing a sixth of worldwide deaths. Cancer is a genetic disease that changes cells phenotype and tissue architecture, inducing localized regions of hypoxia, therefore promoting survival and growth of tissue stem cells which lead to formation of cancerous lesions [2]. The genetic changes needed to develop cancer can be either inherited (germline mutations) or acquired (somatic mutations) as result of errors in cell division or DNA alteration caused by environmental exposure to different stimuli [3]. One of the main challenges in cancer treatment is the uniqueness of each tumor, which is the result of genetic changes that are different from patient to patient [4]. Cancer cells presents distinct key features, as they are less specialized than healthy cells, they can avoid signals that usually stop cells from dividing or that induced programmed cell death (apoptosis) and can evade the immune system, even using it at their advantage to stay alive and proliferate [5]. In order to survive and proliferate, cancer cells need higher amounts of oxygen and nutrients, so they need to be surrounded by a vascular network. Malignant tumors that rapidly grow are highly vascularized, whereas dormant tumors are not [6]. As cancer cells growth rate is higher than normal cells, the compulsive formation of new vasculature associated with an overexpression of pro-angiogenic factors leads to the development of a disorganized blood vessels network. These blood vessels present structural and functional abnormalities, exhibiting hyperpermeability and no distinction between arterioles, capillaries and venules [7]. In a similar fashion, the lymphatic vessels that surround tumor tissues will typically be dilated, leaky and discontinuous [8]. Once cancer cells start to uncontrollably proliferate, eventually they can spread into surrounding tissues, this process is called metastasis. To initiate metastasis cancer cells must [5]:

- Invade through the extracellular matrix (ECM),
- Intravasate into tumoral vasculature, surviving during the transport,
- Extravasate inside the parenchyma of distant organs,
- Survive by manipulating microenvironment and grow into macrometastases.

Metastatic cancer is responsible of 90% of cancer-related deaths [9]. The ideal cancer treatment would be able to destroy selectively as many cancer cells as possible, leaving healthy cells and tissues unharmed.

1.1.1 Traditional therapies in cancer treatment

Cancer treatment strongly depends on cancer type and its progression stage. Each treatment has advantages, disadvantages and limitations. The main available treatments options are:

- Surgery [10], it is the first method that has been employed in history. Its aim is to remove as much of the tumoral mass as possible. The main drawback is that surgery is not suitable for the treatment of metastatic tumors. Moreover, surgeries may leave tumor cells that are found around the edges of the tumor. For this reason it is often associated with other therapies such as radiotherapy and chemotherapy. Moreover, the removal of an organ may affect the patients' quality of live.
- Radiotherapy [11], it employs high energy radiation to kill cancer cells by inducing DNA damage. This therapy is limited by the maximum tolerated dose to healthy tissues that surround the tumoral mass.
- Chemotherapy [12], it involves the use of anti-cancer drugs, traditionally cytotoxic agents that interferes with cell division. The main drawback of chemotherapy is the damage to healthy cells, especially the ones that divide rapidly, which are therefore more sensitive to anti-mitotic drugs.
- Immunotherapy [13], it is based on the modulation of the patients' immune system. However, response to this treatment is patient-specific. Another limitation is imposed by the scarce number of known tumor-specific antigens that can be targeted.
- Targeted therapy [14], it involves the use of drugs or other substances designed for specific molecular targets that are involved in various cancer processes like growth, progression and metastasis. Examples of this kind of therapy are hormone therapies, apoptosis inducers and angiogenesis inhibitors. The main limitation is represented by the fact that tumors usually develop resistance against those agents, through mutations of the target molecules or by finding new pathways to achieve the same results.

1.1.2 Application of nanomedicines in cancer treatment.

Traditional chemotherapy has different limitations such as short half-life, scarce drug solubility, lack of specificity of the treatment, cytotoxicity and finally the occurrence of multi-drug resistance (MDR) [15]. The use of nanotechnology-based drug delivery systems, such as nanoparticles (NPs), may overcome these limitations. For example, to overcome lack of specificity in traditional treatments, NPs rely on two targeting mechanisms: passive and active targeting. A schematic representation of both mechanisms is reported in Figure 1.

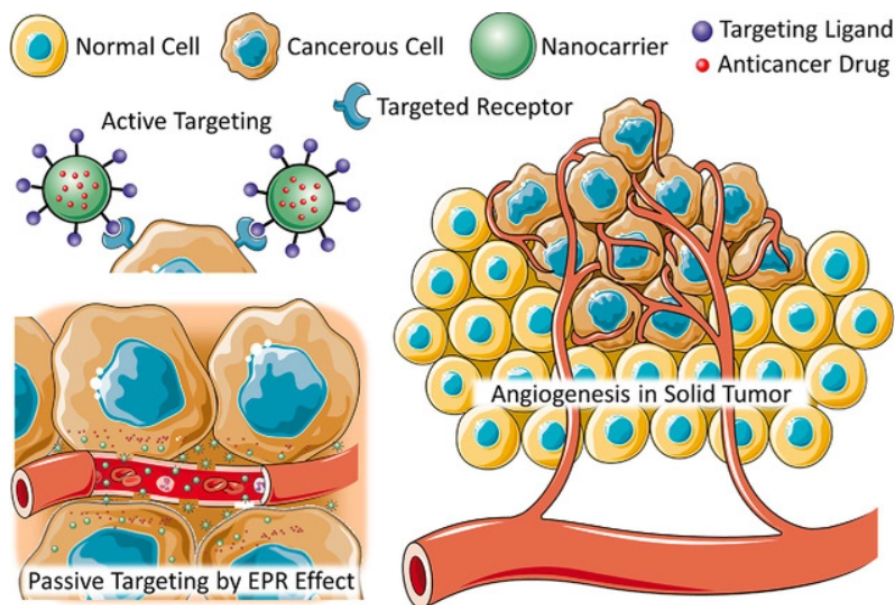


Figure 1: Schematic representation of passive and active targeting [16].

Passive targeting exploits the enhanced permeability and retention (EPR) effect, which was first observed by Maeda et al. [17]. As mentioned before, both tumor blood and lymphatic vessels are abnormal, the first one presenting higher permeability than healthy blood vessels, the second lacking proper drainage. Due to EPR effect nanoparticles with appropriate characteristics, for example small size (in the range of 100-200 nm) and high circulation time, can leak through the impaired vasculature and remain trapped as a consequence of the improper drainage [18]. Despite being an appealing mechanism, therapies cannot always rely on EPR as it depends on the tumor stage, its location and its subtype, for example, therapies against pancreatic cancer can not rely on the EPR effect. Furthermore, nanoparticles should be able to evade clearing organs such as liver and kidneys. On the other hand, active targeting is based on the interaction between specific antigens

or receptor overexpressed or only expressed by tumor cells and the nanoparticles' surface [19]. This mechanism can be achieved by conjugating ligands on the surface of the nanoparticles that act as targeting molecules. To take full advantage of active targeting, proximity of the nanoparticles to the tumor tissues is required. This can be achieved by combining passive and active targeting [20]. In addition, ligands can also target intravascular tumor cells or even endothelial cells of tumor blood vessels, in order to promote nanoparticles' accumulation within the desired site [19].

NPs are nanostructured drug carriers that possess at least a characteristic size in the range between 1 and 400 nm and can be classified according to their size, shape and composition [21]. Depending on the material they are composed of nanoparticles can also be divided into:

- Lipid based nanocarriers: they can be either massive solid lipid nanoparticles or hollow (liposomes), with at least one phospholipid bilayer that forms a hollow sphere entrapping drugs [22].
- Inorganic nanoparticles: they can be iron oxide, silicon oxide, gold nanoparticles or quantum dots [23], mostly used for imaging and diagnosis rather than for drug delivery.
- Polymer based nanocarriers: they typically are massive nanoparticles [24]. Depending on the polymer used, nanoparticles can encapsulate both hydrophobic and hydrophilic drugs. The polymers used for polymeric NPs are usually biocompatible and biodegradable. Moreover, the surface can be modified with functional groups for active targeting [25].
- Hybrid nanoparticles: they are synthesized using both lipids and polymers. Typically presents a shell-core structure and are designed to exploit the most favorable characteristics from both polymeric systems and lipidic systems to overcome their disadvantages [26].

Nanoparticle formulations demonstrated to improve bioavailability by incrementing aqueous solubility, and to increase half-life of target drugs [27]. One of the major limitations after injection is the nanoparticles sequestration by the mononuclear phagocyte system. This preceded by a process called opsonization that consists in the absorption of plasma proteins onto the surface of nanoparticles [28]. Polyethylene glycol (PEG) coatings is the most used method to augment circulation time of nanoparticles. PEG, or polyethylene oxide (PEO) is a polyester widely used in medicine for its "stealth" properties and its safety in humans, being classified

as Generally Regarded as Safe (GRAS) by the FDA [29]. PEG chains generate a hydrated cloud that sterically protects nanoparticles from aggregation and from interaction with blood components [29], thus impeding the opsonization process.

In literature many examples of advanced drug delivery systems can be found. Most notably, drug formulations like Doxil® and Abraxane® are the first marketed nanomedicines that exploit advanced drug delivery systems. The first being a liposomal formulation of doxorubicine, the latter being based on albumin-bound paclitaxel. In particular, Doxil®, represents one of the most successful uses of PEGylation, in which the drug lifetime was increased from minutes to hours [30].

1.2 Microtubules

Microtubules, shown in Figure 2, alongside actin and intermediate filaments, constitute the cell's cytoskeleton. The cytoskeleton is the structure that provides shape, stability, internal organization and mechanical support to eukaryotic cells. Microtubules are dynamic polymeric structures made of repeating subunits, a globular protein called tubulin. Tubulin is a dimer, formed by α -tubulin and β -tubulin, which are about 40% identical at the amino acid level, they weigh approximately 55 kDa [31]. Tubulin subunits are assembled to form a rigid, hollow, cylindrical protein composed of α/β -heterodimers. The tubulin heterodimers assemble in a head-to-tail fashion to form the protofilaments (13 in most cells), which associate longitudinally to form a sheet, which then closes to form a microtubule with an external diameter of 25 nm, an internal diameter of 14 nm and length up to 50 μ m. Microtubules have two different ends:

- α -tubulin is exposed at the less dynamic end (minus end), which anchors the microtubules to the microtubule-organizing center (MTOC).
- β -tubulin is exposed at the more dynamic end (plus end), exposed to the cell periphery.

γ -tubulin is a third type of tubulin that is found in the centrosome and plays an important role in starting the microtubule assembly from the minus end. Microtubules exert different functions such as influencing cell shape and movements, intracellular trafficking of macromolecules and organelles and accurate chromosome separation, playing a crucial role in mitosis, which makes them suitable as target for anticancer therapies [32].

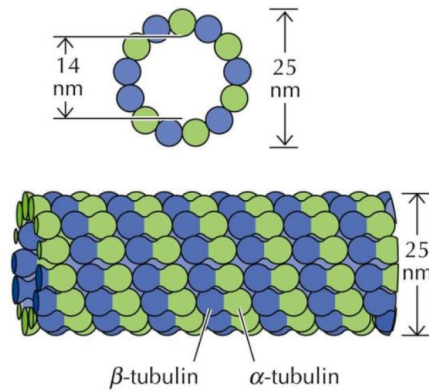


Figure 2: Microtubule structure. From THE CELL, Fourth Edition, Figure 12.42.

1.2.1 Microtubules Dynamics

Microtubules are very dynamic structures, due to their unique guanosine-triphosphate (GTP) binding and hydrolysis properties. This mechanism is characterized by the interaction of both α -tubulin and β -tubulin with GTP, a nucleotide analogous to ATP, that releases energy when hydrolyzed in guanosine-diphosphate (GDP). Both α -tubulin and β -tubulin can bind GTP, however, β -tubulin can also bind GDP. When the GTP binds to β -tubulin, it becomes hydrolyzed GDP. The tubulin binding affinity with the nearby tubulins weakens, stimulating depolymerization of the microtubules. The balance between the addition rate of GTP-bound tubulin and GTP hydrolyzation rate determines the growth rate of each end [33].

Microtubules show two distinct properties:

- Dynamic instability, which is described as the stochastic alternation between episodes of growth (rescue) and shortening (catastrophe) of microtubules [34]. A schematic representation of dynamic instability is reported in Figure 3.
- Treadmilling, as one end of the microtubule presents a net growth, and the opposite end presents a net shortening [33].

The dynamic properties of microtubules are pivotal for many cellular functions. The most attracting one for drug development is the proper spindle functioning during mitosis. Spindle microtubules are 10 to 100-fold more dynamic than interphase microtubules, to enable efficient capturing, alignment, and segregation of chromosomes. Suppressing microtubules dynamics impairs successful chromosome attachment and movement, blocking cell cycle progression at mitosis [33].

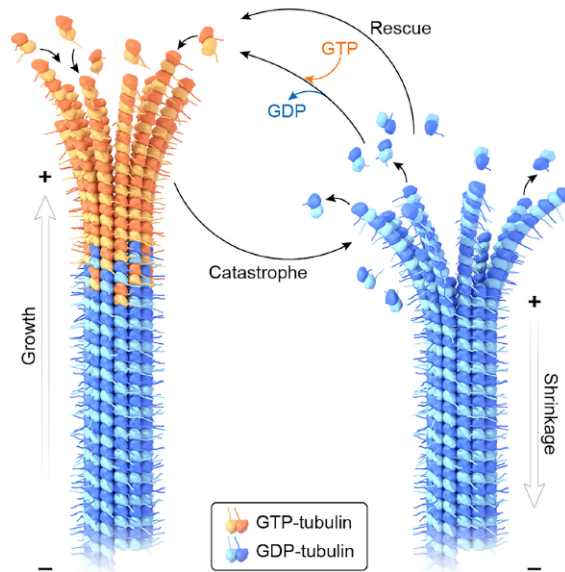


Figure 3: Dynamic instability representation, growth (rescue) and depolymerization (catastrophe) cycles are highlighted [34].

1.2.2 Tubulin isotypes

Looking at tubulin isotypes, they share a high degree of sequence homology and can be distinguished by highly divergent sequences at the level of the carboxy-terminal tail [35]. However, α -tubulin has shown a higher conservation, hence β -tubulin isotypes have been the most appealing to study. Ten β -tubulin isotypes have been discovered: β I, β IIa, β IIb, β III, β IVa, β IVb, β V, β VI, β VII and β VIII [31]. The isotype expression of β -tubulin in normal and tumoral tissues has been studied over the years. In normal tissues, β I, β IVb and β V are ubiquitous, β VI is hematopoietic cell-specific, while β IIa, β IIb, β III and β IVa are neuronal cell-specific [36]. The role of different β -tubulin isotypes has been extensively studied but the correlation between alterations in β -tubulin isotypes and drug resistance to Microtubule-Targeting Agents (MTAs) remains unclear [37].

1.2.2.1 β III-tubulin expression in cancer

One of the most overexpressed tubulin isotypes in cancer cells is β III-tubulin, which is thought to play a role in antimetabolic drug resistance [38]. Other characteristics such as more pronounced tumor aggressiveness, tumor differentiation and lymphatic metastasis are associated to β III-tubulin expression [37]. Resistance to MTAs as

consequence of β III-tubulin may be explained by different mechanisms:

- Increased microtubule dynamic instability: β III-tubulin isotype forms the most dynamic microtubules [39]. This enhancement lead to resistance to MTAs, reducing for example their ability to suppress microtubule dynamics in some cases [40]. This mechanism, however, still remains unclear [37].
- Reduced drug-tubulin interaction: some MTAs such as vincristine and vinorelbine demonstrated to have lesser binding affinity to β III-tubulin when compared with other isotypes [41]. On the other hand, compounds that bind to the colchicine-site of the β -tubulin show no difference in binding affinity [42].
- Inhibition or evasion of drug-induced cell death: it is thought that β III-tubulin is involved in mitotic slippage, a key mechanism of cancer cell resistance to MTAs-induced apoptosis [43], by regulating the caspase-mediated apoptotic cascade in tumoral cells [44].

In some instances, β III-tubulin overexpression has been associated with increased survival of patient affected by malignant melanoma and in better responses to taxane-based chemotherapy in breast cancer and ovarian clear cell adenocarcinoma [37]. Given the different roles played by this protein, it is extremely important to assess its functions in a given tumoral tissue.

1.2.2.2 Strategies to overcome β III-tubulin overexpression

Different strategies, summarized in Figure 4, have been developed to overcome the negative effects of this tubulin isotype in cancer progression:

- Nanoparticles-based approaches were studied, both using miRNA-200c [45] and different MTAs [46]. Suppression of β III-tubulin expression using miRNA showed promising results as it restored cancer cells sensitivity to MTAs [45]. MTAs' nanoformulations can enhance cellular delivery and therefore efficacy, however if these formulations plays a role in overcoming β -III tubulin-mediated drug resistance has to be determined [37]
- The use of small-molecules has been studied to affect components that regulates β III-tubulin expression. For instance, VERU-111, an orally available MTA that binds to the colchicine site on β -Tubulin showed good anti-proliferative and anti-metastatic effect both *in vitro* and *in vivo* [47]

- The use of antimicrobial peptides demonstrated to affect colon cancer metastasis both *in vitro* and *in vivo* [48].
- The use of covalent tubulin-binding agents such as pironetin has shown promising effects that could overcome β -III tubulin-mediated resistance in cancer cells [49]. This compound covalently binds to α -tubulin and perturbs secondary structures located at the interdimer interface, completely evading β III-tubulin-mediated drug resistance. Moreover it has shown higher efficacy in β III-tubulin expressing cells, even at nanomolar concentration [49].
- The use colchicine binding MTAs can effectively avoid β III-tubulin-mediated drug resistance, as their binding affinity is not reduced by the overexpression of the β III-tubulin isotype [42].

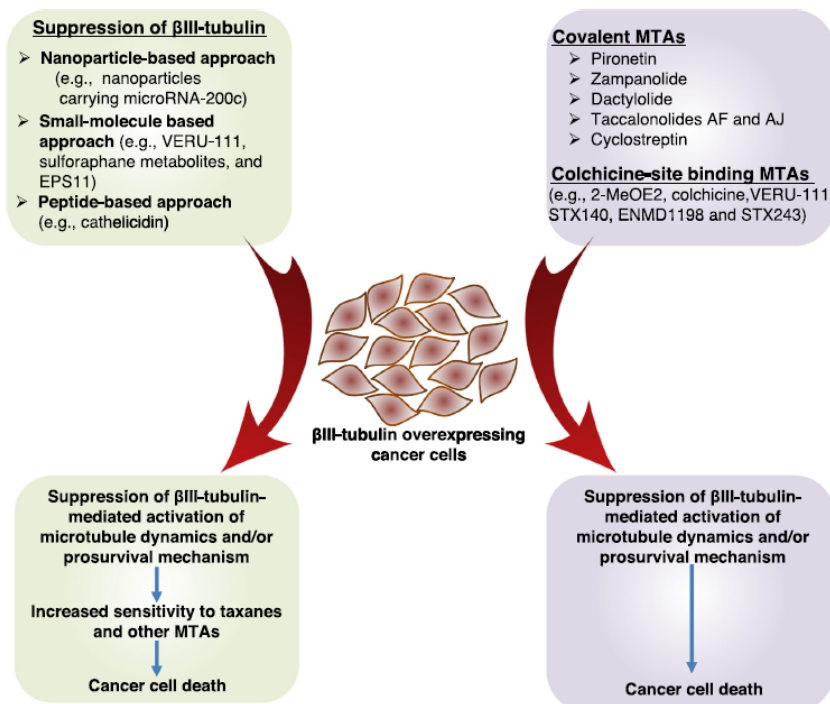


Figure 4: Overview on the strategies to overcome β III-tubulin overexpression, [37].

1.3 Microtubules-Targeting Agents

Microtubule-Targeting Agents (MTAs) are a group of chemical compounds capable of interfering with the dynamic behavior of microtubules upon binding to α -tubulin or β -tubulin, although most of the known MTAs bind to β -tubulin. The first classification of these drugs is based on their mechanism of action, as they can stabilize (microtubules-stabilizing agents, or MSAs) or destabilize (microtubule-destabilizing agents, or MDAs) tubulin. It has been demonstrated that MTAs mechanism of action depends on their concentration. At low concentrations microtubules become less dynamic, regardless of whether MDAs or MSAs are used. On the other hand, when the concentration increases changes in the total microtubular mass (increases for MSA and decreases for MDA) have been observed [50]. In the past it was thought that three binding-sites were present in tubulin (taxane binding-site, vinca domain and colchicine binding-site), but the most recent discoveries report up to seven sites, two in α -tubulin and five in β -tubulin [51].

- Taxane site (red in Figure 5), located in the β -tubulin monomer towards the microtubule's lumen. Taxanes are microtubules-stabilizing drugs [52].
- Vinca domain, (orange in Figure 5), located in the β -tubulin monomer. Drugs that bind to this site, like vincristine, vinblastine and vindesin can inhibit tubulin assembly by forming paracrystalline tubulin aggregates [53].
- Colchicine site (cyan in Figure 5), which is present in β -tubulin at the interface between α - and β -tubulin. Drugs that bind in this site induce a conformational change in tubulin which prevents further microtubule formation [54].
- Maytansine domain (green in Figure 5), it is located next to the vinca site. Drugs that bind in this site are considered as microtubule-destabilizing agents [55].
- Laumalide/peloruside site (magenta in Figure 5), located in a pocket of β -tubulin facing the outside of the microtubule. Drugs that bind this site inhibit microtubule disassembly by holding together protofilaments, with molecular "clamping" action [56].
- Pironetin site (blue in Figure 5) is the first site present in α -tubulin that has been discovered, it hosts destabilizing agents that inhibits tubulin-tubulin interactions at the microtubules cap [57].

- Gatorbulin site (yellow in Figure 5) is the most recently discovered site. It is present in α -tubulin at the interface between α - and β -tubulin. Drugs that bind in this site have a similar mechanism to the vinca domain binding agents [58].

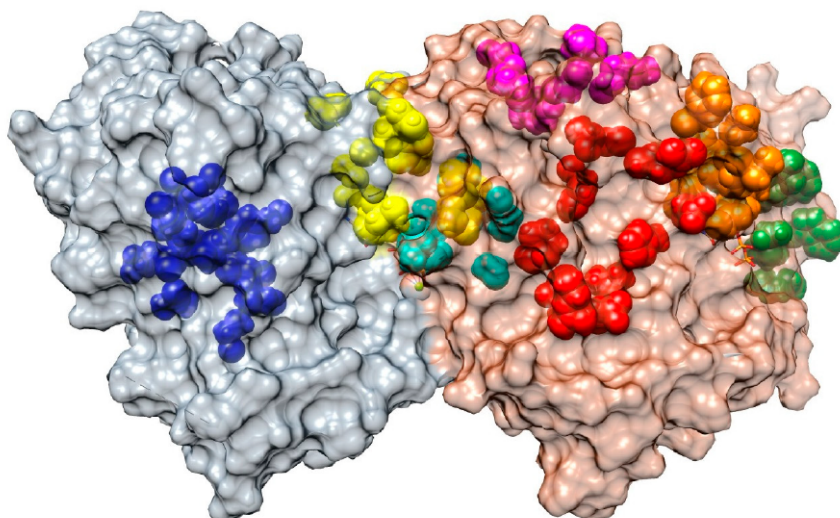


Figure 5: MTAs binding sites on α -tubulin β -tubulin heterodimer. α -tubulin is represented on the left, β -tubulin is represented on the right, [51].

These drugs, mainly taxanes and vinca alkaloid [51], are used to treat cancer since the mid-1960s, whereas the use of colchicine has been restricted to diseases such as gout and Familial Mediterranean Fever due to its high toxicity [59]. MTAs can also serve as herbicides, anti-parasitic, antifungal agents and proved to be useful in neurodegenerative diseases treatment. Other agents that bind to the colchicine site or colchicine derivatives are being studied for the treatment of different tumors [50] to overcome the toxicity issues of colchicine. For example, combretastatins are an appealing group of agents that binds to the same site as colchicine and have shown efficacy in ovarian cancer [60] and lung cancer therapy [61], acting both as antitumoral and anti-angiogenic agents.

1.3.1 MTAs effects on cancer cells

MTAs effects on microtubules dynamics affect cells mitosis leading to cell death [33]. The most well understood mechanism leading to cell death induced by MTAs is the mitotic spindle disruption. As stated above, MTAs can alter chromosome segregation, blocking the cells in metaphase and triggering their death [50]. MTAs

can also prevent metastasis initiation, which requires a change in cancer cells phenotype from epithelial to mesenchymal to acquire migratory and invasive features. Cells then enters the vascular and the lymphatic systems, circulating throughout the entire body and colonizing other tissues. To successfully spread through this mechanism, cancer cells need a functional cytoskeleton, so the use of the MTAs and the subsequent alteration of microtubule dynamics can impair these cellular events.

1.3.2 MTAs effects on tumoral vasculature

Tumors typically exhibit an altered vasculature, due to the high proliferation rate of cancer cells that increases their need of oxygen and nutrients. An impairment in tumor vasculature can indeed lead to tissue necrosis. Moreover, tumor vasculature is needed for metastasis initiation. There are two ways to target vasculature, drugs can either inhibit the formation of new blood vessels (antiangiogenic drugs) or disrupt the already existing vessels (vasculature-disrupting agents, VDAs). MTAs presents both mechanisms, as they impair also endothelial cell proliferation, migration and morphology [51]. These effects can be observed at low drug concentrations, probably because the alterations in microtubule dynamics affect cell signaling pathways, damaging focal adhesions and adherent junctions therefore disturbing cell-cell interactions [62]. A representation of the effects of VDAs and anti-angiogenic drugs is reported in Figure 6.

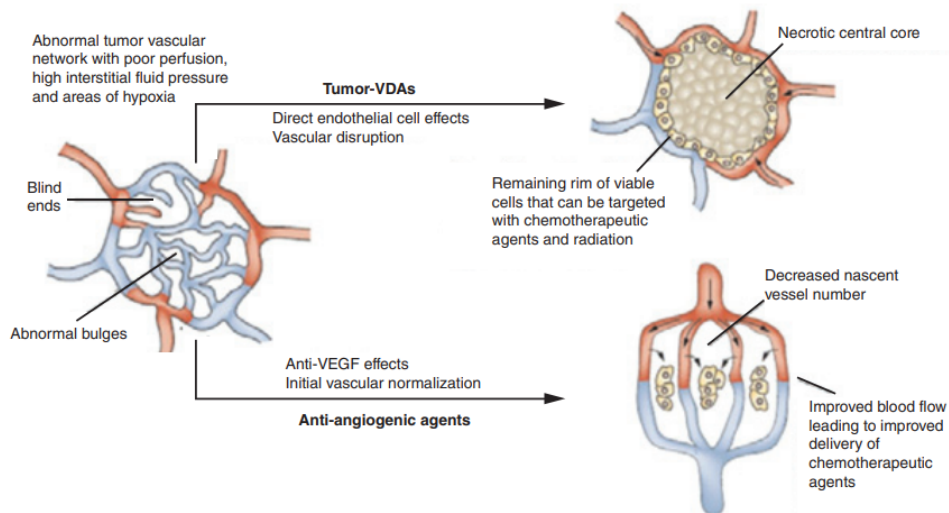


Figure 6: Schematic representation of VDAs and anti-angiogenic drugs mechanisms, [63].

1.3.3 Multi-Drug Resistance in MTAs

Although MTAs represent an interesting class of compounds to treat a variety of cancers, multi-drug resistance can hamper their efficacy. Multi-drug resistance can be classified either as *intrinsic* when it does not depend on exposure to the drug or *acquired* if the mechanism is a consequence of cancer cells exposure to the drug. Moreover, some cancer cells do not respond to MTAs as they feature oncogenic proteins that are independent of microtubules. The most common drug-resistance methods cited in literature are:

- Expression of different isotypes of β -tubulin [51, 33, 50].
- ATP-binding cassette (ABC) transporters [51, 33, 50]

. While the first mechanism has already been discussed in the strategies to overcome β III-tubulin overexpression chapter, the ATP-Binding Cassette transporters are a family of transmembrane proteins which usually transports different types of molecules across the cell membrane. These proteins are powered by ATP hydrolysis and protect the normal cell against potentially harmful chemicals. Therefore, an overexpression of these proteins leads to multi-drug resistance in cancer [64]. The most well studied ABC is the P-glycoprotein 1 (P-gp), which interacts with more than 200 compounds, presenting a flexible molecule-binding site and low specificity. To block P-gp-induced multi-drug resistance different classes of inhibitors have been studied. They can either block the P-gp binding site, interfering with ATP hydrolysis and inactivating the pump, or alter the cell membrane [65].

1.4 Colchicine

Colchicine is an alkaloid compound known for millennia, isolated for the first time in 1820 from the seeds and bulbs of *Colchicum Autumnale* and *Gloriosa Superba*. Its formula is ($C_{22}H_{25}NO_6$) and its molecular weight is 399.44 g/mol. Colchicine chemical structure is reported in Figure 7. Briefly, the main structure is composed of three rings, the rings A and C are the ones involved in anti-tubulin activity. Ring A is a trimethoxy-benzene ring essential for the correct molecule conformation and binding ability. Ring B is a seven-member ring with

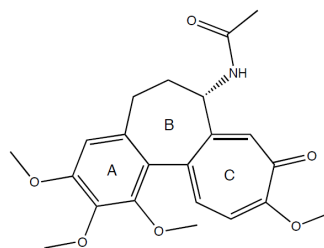


Figure 7: Colchicine chemical structure.

an acetamido group at C7 position, this ring influences conformation of colchicine analogues and their binding properties, as it holds both rings A and C in a rigid conformation. Ring C is a methoxy-tropolone ring, and its purpose is the drug-tubulin interaction, this ring is responsible for the drug photosensitivity as it can be photochemically decomposed. In 2009, colchicine received FDA approval as an anti-inflammatory to treat symptoms of gout and Familial Mediterranean Fever. Colchicine has also been proposed to treat rheumatic conditions like osteoarthritis [66] and Behçet disease [67], cardiovascular diseases like pericarditis and atherosclerosis [68], hepatic diseases biliary and hepatic cirrhosis, and other pathologies such as aphthous stomatitis, chronic urticaria, dermatitis herpetiformis and amyloidosis [66]. Its use as anti-cancer compound has also been investigated [69, 70, 71].

1.4.1 Colchicine mechanism of action

Colchicine interferes with mitosis by disruption of microtubules, its main target is tubulin. In 2004, Ravelli et al. identified the colchicine-binding site at the interface between α -tubulin and β -tubulin that forms the heterodimer [72]. This leads to the formation of the so-called tubulin-colchicine complex (TC-complex), that differs from the normal tubulin by having a curved rather than straight conformation. Once the TC-complex is formed, tubulin can be employed in microtubule polymerization, although it will induce a conformational change preventing further microtubules growth by sterically blocking further addition of other tubulin dimers [51]. This conformational change may be the cause of structural instability that leads to microtubule spindle disassembly at the mitosis metaphase [73]. As common for most of MTAs, colchicine concentration (the quantity of TC-complexes that are incorporated into the microtubules), determines whereas the microtubule stop its growth or starts to depolymerize, respectively at low and high concentrations [74]. Interestingly, colchicine also exhibits antiangiogenic properties and is also capable of destroying existing tumor vasculature, however *in vitro* studies demonstrated that the needed plasma concentration to obtain those effects can be lethal [75] Unfortunately, colchicine has a narrow therapeutic index, this means that the range between therapeutic and toxic doses is small, and occasionally they overlap [59]. In fact, in 2008 FDA banned intravenous administration of colchicine as it caused severe side effects such as tissue necrosis, intravascular coagulation and death [76]. Another limitation of this molecule is its high hydrophobicity, which limits drug solubility and absorption, also reducing the drug entrapment efficacy in different drug delivery

systems []. These problems may be addressed through the production of prodrugs, modification of the colchicine molecule using a Rational Drug Design approach or by using advanced drug delivery systems that can enhance drug solubility, increase permeability and absorption and increase biological half-life.

1.4.2 Colchicine derivatives: CCI-001

As stated before, the main issues of the currently marketed anticancer drugs are the lack of specificity which leads to severe side effects and multi-drug resistance. Colchicine also presents a narrow therapeutic index responsible for its high toxicity. To overcome those limitations, Prof. J. A. Tuszynski and his co-workers developed, through a Rational Drug Design approach, and then synthesized, seventy colchicine derivatives divided in two series (CH and CCI). The aim of their work was to obtain a selective MTA for β III-tubulin with higher toxicity against cancer cell while keeping a low toxicity profile against normal cells. All the compounds were first tested *in silico* and then *in vitro* to assess cytotoxicity, then lead compounds were studied *in vivo*.

Among the seventy compounds tested, three of them showed better results: CH35, CCI-001 and CCI-42-23. Unfortunately, CH35 was not eligible to be patented. Both CCI-001, or CR-42-24, and CCI-42-23 were patentable, but CCI-001 proved to be the lead compound as it showed a superior ADMET profile.

CCI-001 brute formula is $(C_{23}H_{27}NO_6S)$, its chemical structure is reported in Fig. 8 and it shows the following features:

- Molecular Weight: 445.5 g/mol
- Predicted binding free energies (kcal/mol) with respect to major tubulin iso-types:

β I: -53.1	β IIa	β IIb: -39.1	β III: -48.4
β IVa: -32.0	β IVb: -44.0	β V: -63.8	β VI: -47.6

- LogP: 2.58
- Solubility in water at pH 7.4 = 0.007 mg/ml

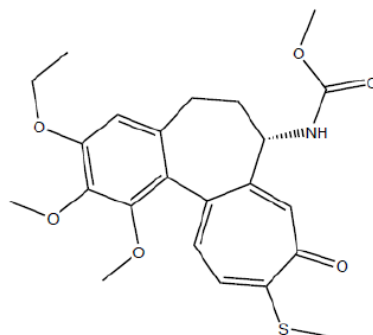


Figure 8: CCI-001 chemical structure.

MTS and MTT assays evaluated cytotoxicity against numerous cancer cell lines, comparable if not higher than the standard of care anticancer compounds available on market. CCI-001 proved to be active on bladder, colorectal, skin, breast, pancreatic and kidney cancer cells with IC_{50} values in the nM scale. Regarding to healthy cells, slight cytotoxicity against GM38 fibroblast cells was observed. CCI-001 was proven to be more effective than paclitaxel in most of the tests. When tested on a panel of bladder cancer cell lines (T24, 253J, UM-UC-3, UM-UC-14) CCI-001 activity was more efficient than gemcitabine and cisplatin, both used as single agents or in combination. CCI-001 was also tested and compared with many marketed MTAs, such as paclitaxel, vinblastine, combretastatin, laulimalide and taccalonolide, to test its efficacy against taxol-resistant cancer cell lines. In this case, CCI-001 was more effective than the other MTAs, although even at high concentrations some surviving cells were found. This resistance may be attributed to P-gp activity. To assess this hypothesis, CCI-001 was tested alongside 3-bromo pyruvate (3BP), a compound that inhibits the P-gp activity [77]. When tested on paclitaxel-resistant SK-BR-3 the compounds showed synergistic ability, since cell viability dropped from 27.9% to 2.1% when CCI-001 was administered alone and with 3BP, respectively. To maximize the synergistic effect 3BP should be administered 3 hours before CCI-001. However, CCI-001 was found to be a weaker substrate to P-gp when compared to colchicine. Other studies investigating synergistic effects between CCI-001 and other anticancer compounds have been performed, showing that CCI-001 may improve the effects of gemcitabine and cisplatin, only when administered in a sequential manner. In particular, with a cell pre-treatment with CCI-001 and subsequent administration of cisplatin or with a cell pre-treatment with gemcitabine and subsequent administration of CCI-001. *In vivo* studies confirmed the promising anti-cancer activity of CCI-001. When tested on T24 xenografts in mice at different concentrations (3 mg/kg or 6 mg/kg) for a period of 10 days, CCI-001 was able to suppress tumor growth without showing pronounced toxicity and 3 mg/kg was found to be enough for tumor growth prevention. When compared to gemcitabine/cisplatin chemotherapy, CCI-001 showed comparable effects a 3 mg/kg, confirming this is a sufficient dose to suppress tumor growth. A clinical trial on CCI-001, intended for patient with recurrent or metastatic solid tumors, is currently ongoing.

Other remarkable features of this novel colchicine derivative are its ability to inhibit migration in primary endothelial cells, thus preventing metastasis, and its anti-angiogenic effects that have been observed in mice. Furthermore, its toxicity is very low compared to colchicine, taxol, gemcitabine and cisplatin and its efficacy

is proven at low concentrations. These results suggest CCI-001 as a valid alternative for the treatment of cancers, especially with acquired or intrinsic multi-drug resistance. Moreover, synergistic effects may further improve CCI-001 effectiveness. The main issue with this compound is represented by its poor water solubility, being 1000-fold less water soluble than its parent compound colchicine, having a solubility in water of 0.007 mg/ml and 7 mg/ml, respectively. The lipophilic character of CCI-001 leads to limited absorption. To fully exploit the potential of this new compound, it is crucial to overcome this limitation, for instance by exploiting different drug delivery system.

1.5 CCI-001 Nanoformulations

Different strategies have been adopted to deliver CCI-001. An Antibody-Drug Conjugate (ADC) of CCI-001 and Panitumumab was produced, however it did not express improved antigen dependent activity of the drug. Albumin/CCI-001 NPs were produced with an average size of ~ 130 nm, narrow size distribution, zeta potential of ~ -30 mV and a EE of 6% [78]. The latter nanoformulation showed good results in in vitro tests. However, the use of a more flexible method that can improve EE and overall efficacy is needed.

1.6 Nanoprecipitation

To obtain the CCI-001 loaded NPs, the nanoprecipitation method (or solvent displacement method), schematically illustrated in Figure 9, was adopted. This method, enticing due to its simplicity, can be used to obtain polymeric NPs, lipidic NPs or hybrid NPs [79], such as the one produced for this work. To perform nanoprecipitation, two miscible solvents are used, one of them has to be a good solvent, the other one has to be a non-solvent for the materials that will form the particles. This method requires the preparation of two phases, an organic phase and an aqueous phase, in which the starting materials are solubilized. The aqueous phase often contains stabilizing agents, while the organic phase can contain polymers, lipids, surfactants and the active molecules, depending on the desired formulation. Multiple solvents in order to modulate the precipitation rates of each component can be used [80]. The aqueous phase generally contains stabilizing agents which allow particle formation and physical stability of the system [81]. NPs will form spontaneously when the organic phase is added dropwise to the aqueous phase while stirring. This happens due to the fast diffusion (displacement) of the organic solvent from the polymeric

core of the particles towards the aqueous phase. NPs are then collected and washed by centrifugation, filtration or using a rotary evaporator [82]. The obtained NPs are generally small ($< 200\text{nm}$) and have a narrow distribution, presenting a PDI lesser than 0.2. The characteristics of the nanosized system will be affected mainly by the nature and concentration of the starting materials [79]. The main limitations of this method are, however, the use of toxic solvents (such as acetone or acetonitrile) and the limitation to hydrophobic drugs.

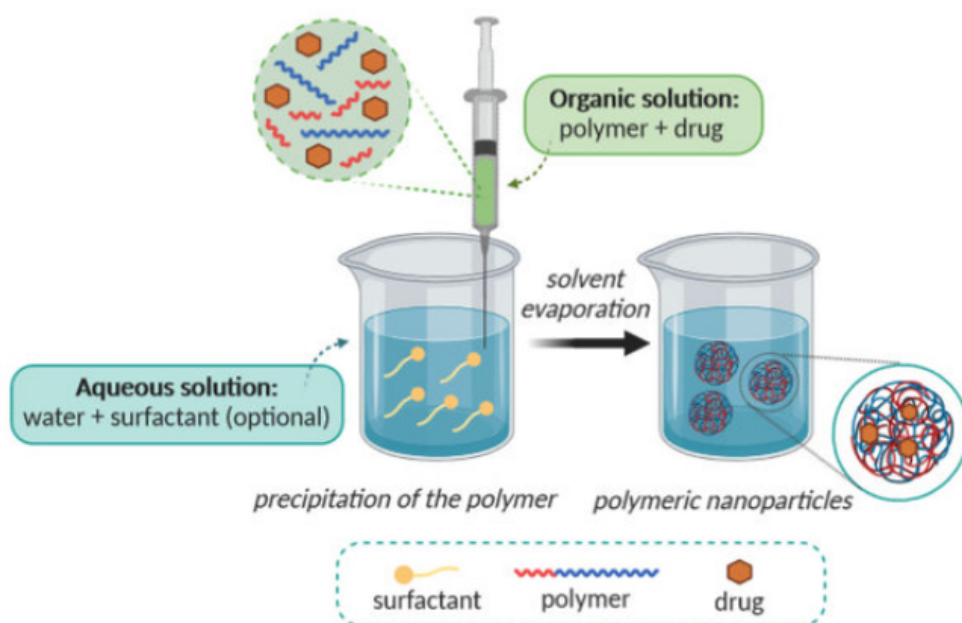


Figure 9: Schematic illustration of the nanoprecipitation, or solvent displacement method.

1.7 Aim of the work

The purpose of this work is to produce self-assembled NPs to improve the delivery of CCI-001. The NPs will be synthesized by nanoprecipitation, and will be composed of a polymeric core, a lipidic monolayer protecting the core (EGG-PG) and a pegylated lipidic shell (DSPE-PEG). CCI-001 is a novel colchicine derivative, synthesized and patented by Professor Tuszynski et al. in the Department of Oncology, University of Alberta, Edmonton, Canada. It acts as a microtubule destabilizing agent and has shown great results both *in vitro* and *vivo*, much to be currently on a Phase I clinical trial. Compared to colchicine, CCI-001 presents higher affinity towards β III-tubulin, which is overexpressed in tumor cells. To maximize drug entrapment in the NPs' core, two different polymers, a commercial polyester widely used to prepare NPs (PLGA) and a polyurethane developed in prof. Ciardelli's lab (NHSC2000), will be used. CCI-001 loaded NPs will be tested *in vitro* against U87MG, a human glioblastoma cell line, and MIA-PaCa-2, a human pancreatic adenocarcinoma cell line. Cytotoxicity was evaluated in 2D cultures and 3D cultures (spheroids), comparing the effect of the free drug and the loaded NPs. Moreover, cell internalization and toxicity of empty particles will also be evaluated.

2 Materials and methods

2.1 Materials

The polymers used were a proprietary poly-caprolactone (PCL)-based polyurethane (NS-HC2000), synthesized in prof. Ciardelli's lab using Poly(ϵ -caprolactone)-diol (2000 g/mol), nBOC Serinol as chain extender, Dibutyl Dilaurate (DBTL) as catalyst, and 1,6 Hexamethylene diisocyanate (HDI), and Poly(D,L-lactide-co-glycolide) (75:25), mol wt 66-107 (PLGA). All materials were purchased from Sigma Aldrich (Italy). L- α -phosphatidylglycerol (EGG-PG), 1,2-Distearoyl-sn-glycero-3-phosphoethanolamine-Poly-(ethylene glycol) (DSPE-PEG) and l- α -phosphatidylethanolamine N-(lissaminerhodamine B-sulfonyl) (Egg-Liss-Rhod PEDSPE-PEG) were purchased from Avanti[®] Polar Lipids. CCI-001 ($C_{23}H_{27}NO_6S$), was provided by the Department of Oncology, University of Alberta, Edmonton, Canada. the shell. All solvents were of analytical grade.

2.2 Instruments

The list of the instruments used during this work and their use is provided in Table 1.

Instrument	Use
Scale (bc, Orma)	Weight all components
Magnetic hot plate stirrer (AREX Digital PRO, VELP [®])	Heat and stir the solutions
Vortex (Zx3,VELP [®])	Promote solubilization and components interactions
Centrifuge (Beckman Coulter Allegra X-30)	Nanoparticles purification
DLS (Litesizer [™] 500, Anton Paar)	Evaluate size and zeta-potential
Freeze dryer (Coolsafe [™] , Scanvac)	Recover Nanoparticles for storage
SEM (TESCAN MAGNA)	Nanoparticles imaging
Incubator (ISCO Micra 9)	Nanoparticles incubation for drug release
HPLC (Thermo Scientific [™] - UltiMate [™] 3000)	Evaluate drug concentrations
Cell incubator (HeraCell [™] 150i)	Cells culture
Confocal microscope (Nikon ECLIPSE Ti2)	Nanoparticles internalization imaging
Fluorecent microscope (ZOE Fluorescent Cell Imager)	Cells and spheroids imaging
Plate reader (Synergy [™] HTX Multi-Mode Microplate Reader [®] .)	Evaluate cells viability

Table 1: List of instruments used.

2.3 NPs synthesis

2.3.1 Nanoprecipitation

The hybrid self-assembled NPs prepared for this study have a core-shell structure. The core is made of NS-HC2000 or PLGA, while the shell is made of a lipid layer of EGG-PG surrounded by the outermost layer, made of DSPE-PEG. The resulting NPs will present a hydrophobic core suitable for the encapsulation of hydrophobic drugs such as CCI-001, and a pegylated lipid surface to impart stealth properties. The NPs were prepared as follows: NS-HC2000 or PLGA and CCI-001 were dissolved separately in ACN at 10 mg/ml and 1 mg/ml concentration respectively, EGG-PG and DSPE-PEG were dissolved separately in a solution of 10% ethanol in distilled water (EtOH-ddH₂O, 10% v/v) at 1 mg/ml concentration.

The organic phase was obtained using 1 ml of ACN solution containing 1 mg of NS-HC2000 or PLGA, the aqueous phase was obtained using 2 mL of ddH₂O containing 240 µgr of DSPE-PEG and 200 µgr of EGG-PG. To obtain drug-loaded nanoparticles, 75 µgr or 100 µgr of CCI-001 were added to the organic phase, whereas to produce fluorescent nanoparticles (Rhod-NPs), 10 µgr of Egg-Liss-Rhod PEDSPE-PEG, a fluorescent lipid, were dissolved in the aqueous phase as a component of the lipid shell of the NPs.

To obtain the nanoparticles, the aqueous phase was stirred gently at 300 RPM and heated to 60°C to aid lipid's solubilization and to avoid micelles formation. Then the organic phase was added dropwise and the obtained NPs suspension was left under stirring at 300 RPM at room temperature for 1h to let the solvent evaporate and the solution cool down. While cooling down 1ml of ddH₂O was added to promote solvent evaporation and temperature reduction.

The obtained nanosuspension was centrifuged using Amicon[®] ultra centrifugal filter units (10 kDa cutoff-membrane) for 13 min at 3200 rpm, 25°C. After that, 1 ml of ddH₂O was added to each filter and a second centrifugation step was performed with the same parameters. The nanoparticles were redispersed in 1 ml of water and stored at -20°C for further characterizations.

2.3.2 Nanoprecipitation - Modified Protocol

The simple nanoprecipitation protocol was modified to enhance drug-polymer interactions before nanoprecipitation. Briefly, the polymer and the drug were mixed vigorously for 3 minutes in ACN and then the solvent was left to evaporate overnight.

A thin yellow polymer film was obtained. The film was redispersed in 1 ml ACN and used as the organic phase in the previously described protocol. Fig.10 summarizes both protocols.

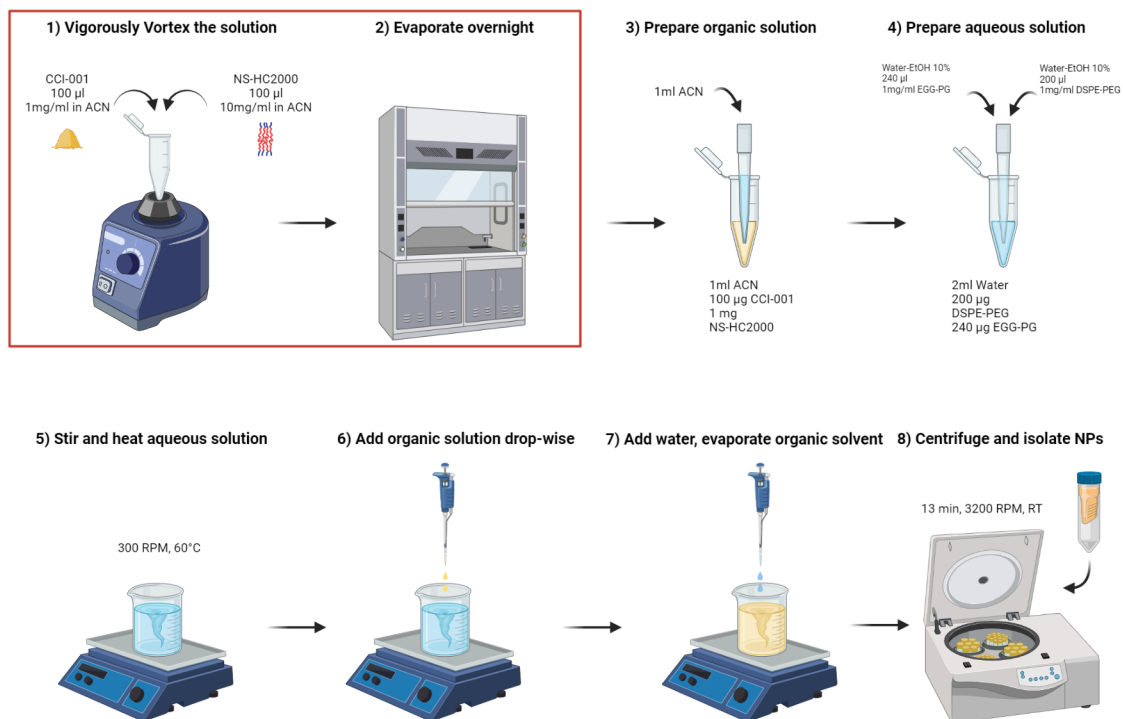


Figure 10: Nanoprecipitation protocol; Step 1 and 2 are added for the modified protocol. Illustration created with BioRender.com.

2.4 Characterization Methods

2.4.1 Size and Zeta Potential

NPs size and zeta potential (ZP) were analyzed using Dynamic Light Scattering (DLS). DLS measures the Brownian motion of particles in a dispersion and uses this information to determine their hydrodynamic size. The instrument irradiates the NPs with a laser and then measures the scattered light intensity. The aforementioned intensity fluctuates creating a dynamic signal, which is rapidly acquired. Through the autocorrelation function of the intensity signal the translational diffusion coefficient is obtained, which is used in the Stokes-Einstein equation with other fixed variables such as temperature and solvent viscosity. In this way, the hydrodynamic diameter is obtained. The hydrodynamic diameter is not the exact physical nanoparticle diameter as in colloidal suspensions it is considered the diameter of a solid sphere that diffuses at the same rate as the sample analyzed. This parameter comprises the core as well as adsorbed molecules on the surface of the NPs, and it is affected by many factors including morphology, core size, and surface properties. Polydispersity Index (PDI) is a parameter that measures the size range of a nanoparticles solution and ranges from 0 to 1 (0 being a perfectly monodispersed sample, 1 for a completely polydispersed sample). For polymeric nanoparticles, values of 0.3 and below are generally deemed acceptable [83]. Zeta Potential (ZP) is defined as surface charge of the particles in a colloidal suspension. The higher the magnitude of the ZP, the lesser are the chances for the particles to agglomerate. Generally ZP values of more than 30 mV in absolute value are considered indicative of a stable solution [84]. NPs Hydrodynamic Diameter, PDI and Size Distribution were measured with the Litesizer™500, Anton Paar, using disposable cuvettes, while ZP was measured using the dedicated Litesizer™ Omega cuvettes (polycarbonate case with gold electrode). For each analysis, the formulation was redispersed in 1 ml ddH₂O in the appropriate cuvette. DLS was used to compare size, ZP, PDI and size distribution between blank and loaded NPs and between the two different protocols. Moreover, to evaluate a proper storage method we tested NPs stability in ddH₂O at 4°C. CCI-001-NSHC2000 NPs were used for this test, size and zeta potential were measured at 0h, 24h, 48h, 72h, 144h and 168h.

2.4.2 Drug Entrapment Efficacy and Drug Release

To evaluate drug entrapment efficacy (EE%) CCI-001 was recovered from the NPs. Two initial loading of CCI-001 were tested (75 μgr and 100 μgr). Freeze dried nanoparticles were dissolved in 200 μL of ACN and vortexed vigorously to break the polymeric core and solubilize the drug. The supernatant was then collected, and the samples were analyzed using HPLC. EE% was calculated as follows:

$$EE\% = \frac{\text{Recovered Drug Amount}(\mu\text{g})}{\text{Starting Drug Amount}(\mu\text{g})} \% \quad (1)$$

For cumulative release studies, NPs' were dispersed in 1 ml ddH₂O and incubated at 37°C. At each time point (0h, 3h, 5h, 24h, 48h, 72h and 144h), the suspension was centrifuged and the supernatant was collected and analyzed. The NPs' were resuspended in 1 ml of fresh ddH₂O and incubated at 37°C. The release percentage was calculated on the percentage of the cumulative release results after 144h (7 days). Drug concentration in each sample was quantified using a Thermo Scientific™ - UltiMate™ 3000 HPLC system. Mobile phase was an isocratic mixture of water and acetonitrile (30:70). The flow rate was set at 1 mL/min at room temperature and the detection wavelength was 286 nm. The assay was found linear over the examined range of 0-20 $\mu\text{g}/\text{mL}$ in the mobile phase, with a calibration curve of equation $y = 0.4854x + 0.4167$ shown in Figure 11. The correlation coefficient R^2 was found to be 0.992. The calibration curve was obtained by analyzing eleven samples as shown in Table 2.

Sample	CCI-001 Concentration ($\mu\text{g}/\text{mL}$)	Sample	CCI-001 Concentration ($\mu\text{g}/\text{mL}$)
Sample 1	1	Sample 7	12.5
Sample 2	2	Sample 8	15
Sample 3	2.5	Sample 9	17.5
Sample 4	5	Sample 10	20
Sample 5	7.5		
Sample 6	10		

Table 2: Samples used to plot the calibration curve

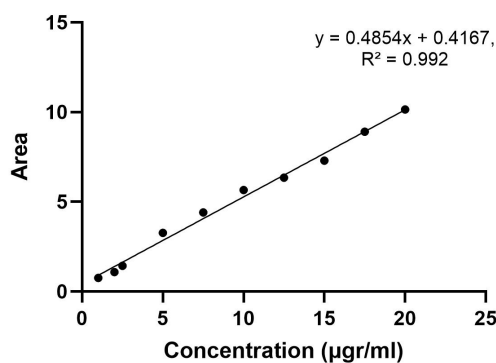


Figure 11: Calibration curve for HPLC, curve equation and R^2 value are shown.

2.4.3 Yield

To evaluate the process yield ($Y\%$) all the formulations were freeze dried. $Y\%$ was calculated as follows:

$$Y\% = \frac{\text{Recovered Formulation (mg)}}{\text{Starting Formulation (mg)}} \quad (2)$$

Starting formulation consists in the sum of polymer, lipids and drug weights. First, empty eppendorf tubes were weighted and then filled with NPs suspension and freeze dried. Eppendorf tubes containing the powdered formulation were weighed again and the yield was calculated by subtracting the eppendorf's weight from the loaded eppendorf weight (recovered formulations).

2.4.4 Morphology

To assess nanoparticles morphology we used a scanning electron microscope (SEM), TESCA MAGNA with its TESCA Essence™ software. A drop of NPs' suspension was placed on taped stubs to proceed with the samples metallization. The samples were coated with a 6 nm thick gold coating and stored at room temperature.

2.5 In Vitro Studies

To evaluate drug efficacy, U87 MG (American Type Culture Collection, ATCC® HTB14™), fluorescent U87 cells transfected to express green fluorescent protein (U87MG-GFP) and MiaPaca-2 (American Type Culture Collection, ATCC® CRL-1420™) were used.

2.5.1 Cell culture

All cell lines were first thawed at room temperature. U87MG or U87MG GFP cells were grown in Gibco™ Minimal Essential Medium (MEM) supplemented with 10% fetal bovine serum (FBS, Gibco™) and 1% penicillin/streptomycin (Gibco™). MiaPaCa-2 cells were grown in Gibco™ Dulbecco's Modified Eagle Medium (DMEM) supplemented with 10% fetal bovine serum (FBS, Gibco™) and 1% penicillin/streptomycin (Gibco™). Both cell lines were expanded in T75 flasks and incubated under standard conditions (37 °C, 5% CO₂), then were plated in 96-well plates (10,000 cells/well) and allowed to attach for for 24h before treatment.

2.5.2 Spheroid culture

Tumour spheroids were obtained in ultra-low attachment U bottom plates (Thermo Scientific™ Nunclon™ Sphera™ 96-Well, Nunclon Sphera Treated, U-Shaped Bottom Microplate) with U87 cells. Spheroids were grown in Gibco™ minimal essential medium (MEM) supplemented with 10% fetal bovine serum (FBS, Gibco™), 1% penicillin/streptomycin (Gibco™). After expansion, U87 cells were plated at 4,000 cells/well with 100 µl of culture medium for each well and then allowed to form spheroids for 4 days.

2.5.3 Citotoxicity evaluation

Cells and spheroids were treated with free CCI-001 and CCI-001-loaded NPs at the concentrations of 1 nM, 10 nM, 20 nM, 50 nM ,100 nM for 24h, 48h, and 72h. Untreated cells and spheroids were used as controls. Cells images at each time point were captured using a ZOE Fluorescent Cell Imager microscope. MTS assay were performed using the CellTiter 96® AQueous One Solution Cell Proliferation Assay, which contains a tetrazolium compound [3-(4,5-dimethylthiazol-2-yl)-5-(3-carboxymethoxyphenyl)-2-(4-sulfophenyl)-2H-tetrazolium, inner salt; MTS] and an electron coupling reagent (phenazine ethosulfate; PES). The MTS tetrazolium compound is bioreduced by cells into a colored formazan product that is soluble in tissue culture medium, in a concentration that is proportional to the number of living cells in the well[85]. 20 µL of CellTiter 96® AQueous Reagent were added to the wells containing cells, in 100 µL of culture medium. The cells were then incubated for 3 hours and the absorbance was read at 490 nm. Cell viability was expressed as a percentage of the absorbance value determined for untreated controls. To assess *in vitro* cytotoxicity for spheroids, CellTiterGlo® 3D Cell Viability Assay (Promega) was used.

This assay uses a thermostable luciferase (Ultra-Glo™ Recombinant Luciferase) that generates a luminescent signal quantifying the adenosine-triphosphate (ATP) presence, which is an indicator of the cellular metabolic activity, by consuming it. The assay also provides a lysis agent that induces the rupture of cell membranes allowing ATP release. 100 μ L of CellTiter-Glo® 3D Reagent were added to the wells containing cells (in 100 μ L), then the contents of each well was transferred to a 96-well opaque white plate for luminescence measurement. The plate was allowed to shake at 410 rpm for 10 minutes to remove bubbles in the same plate reader (Synergy™ HTX Multi-Mode Microplate Reader) used to quantify the luminescent signal. Spheroids viability was expressed as a percentage of the luminescence value determined for untreated controls.

2.5.4 Internalization and infiltration evaluation

Another important factor to consider is cell internalization to verify drug delivery efficacy. Rhod-NPs were synthesized and administered to 2D and 3D U87MG cell cultures, to assess nanoparticles internalization in cells and infiltration in spheroids, respectively. For cells' internalization different NPs concentrations corresponding to 100 nM, 1 μ M and 100 μ M were administered to U87MG GFP 2D cell culture and observed after an incubation period of 24h using a Nikon ECLIPSE Ti2 fluorescent microscope. For spheroids infiltration, a qualitative analysis of this phenomena has been conducted by administration of Rhod-NPs at two different concentrations corresponding to 50 nM and 100 nM to U87MG GFP spheroids that were then incubated for 48h and 72h. After incubation, z-stack imaging was performed using a Nikon ECLIPSE Ti2 fluorescent microscope, in this way spheroids were divided in slices along a z-axis and an image for each slice was taken. Two different types of images were obtained by processing those images:

- Superimposed images were obtained by merging all the slices. Those images are useful to immediately see NPs presence on or inside the spheroids. However, those images do not give information about the NPs exact location.
- Projection images were obtained by analyzing a single slice, selecting a single point and then reconstructing both frontal and lateral projections using all the slices acquired. These pictures are less immediate to analyze but can point out the actual location of the NPs inside the spheroids.

3 Results and discussion

3.1 Nanoparticles Characterization

3.1.1 Size, PDI and Zeta Potential

Size, PDI, and zeta potential of loaded and un-loaded PLGA and NSHC2000 NPs are reported in Figures 12, 13. As expected, a size increase was observed for the CCI-001-loaded NPs, by almost 40nm, suggesting successful loading of the drug. PLGA NPs (160-200nm) appeared to be slightly bigger in size than NSHC2000 NPs (130-170 nm). Both NPs sizes were suitable to exploit the EPR effect (150-200 nm) [28]. All formulations showed narrow size distribution (Figure 12, panels c), d), e) and f)), presenting PDI values below 0.3. PDI values increased after drug loading, ranging from 0.1 to 0.25 for NSHC2000 and from 0.2 to 0.25 for PLGA (Figure 12, panel b)). Zeta potential, shown in Figure 15, increased in magnitude from -24 mV to -30 mV after NPs' drug loading for both NSHC2000 and PLGA. The negative zeta potential represents another advantage since negatively charged NPs are usually internalized more easily by cells through endocytosis [86].

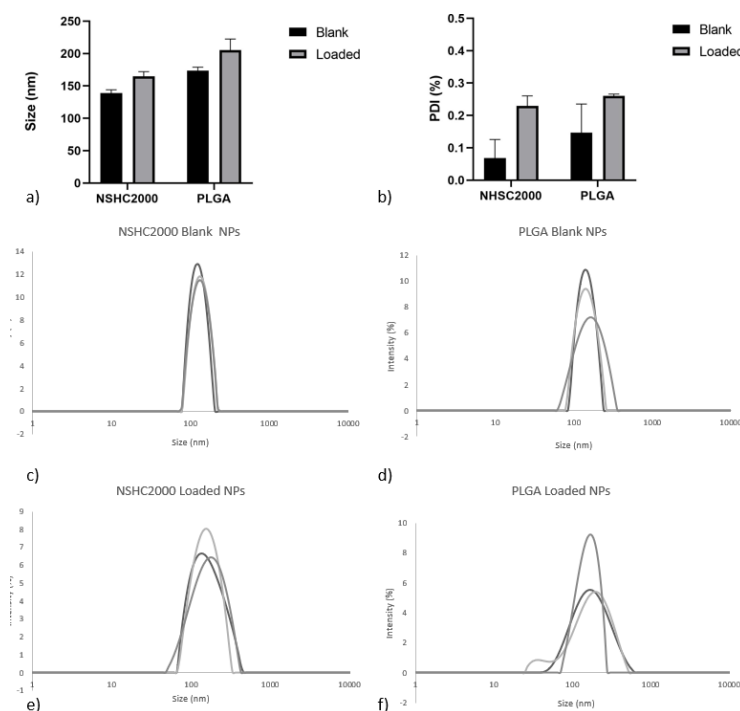


Figure 12: a) Size, b) PDI and size distribution c),d),e), and f) comparison between NSHC2000 and PLGA blank/loaded nanoparticles.

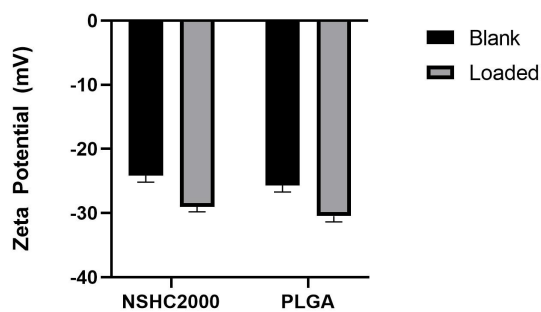


Figure 13: Zeta Potential comparison between NSHC2000 and PLGA blank/loaded nanoparticles.

When the protocols were compared, no difference was observed both for size and PDI, whereas ZP further increased in magnitude from -30 mV to -34 mV, as shown in Figures 14, 15.

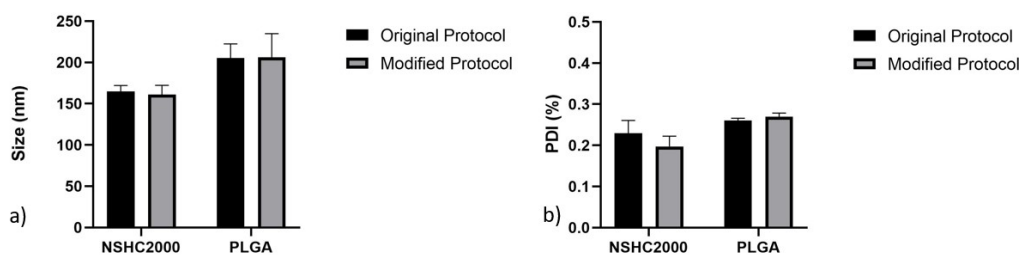


Figure 14: a) Size and b) PDI comparison between NSHC2000 and PLGA nanoparticles obtained with different protocols.

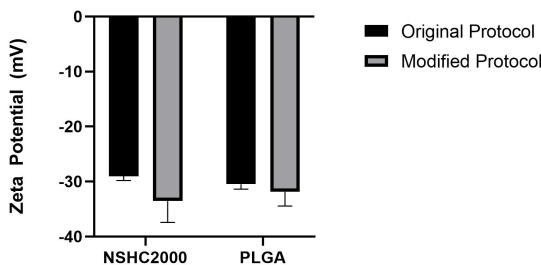


Figure 15: Zeta potential comparison between NSHC2000 and PLGA nanoparticles obtained with different protocols.

3.1.2 Drug Entrapment Efficiency

Drug Entrapment Efficacy was calculated using HPLC, a comparison between the EE% obtained with the two protocols is reported in Figure 16. Modification in the protocol led to an overall increase in EE%, however this increase was marginal for PLGA (from $\sim 1\%$ to less than 2% for both initial loadings). More pronounced increases were observed in NSHC2000 NPs, with an increase from $\sim 1\%$ to 2% and 5% for $75\ \mu\text{gr}$ and $100\ \mu\text{gr}$ initial loadings, respectively. For this reason, NSHC2000 NPs with an initial loading of $100\ \mu\text{gr}$, which reach the amount of $\sim 5\ \mu\text{gr}$ of CCI-001 for each NPs formulation, were chosen for further tests. This result, due to the peculiar properties of CCI-001 (small size and high hydrophobicity) was comparable to other studies performed on the same drug. Further studies involving modifications of other process parameters (i.e. effect of pH) may further enhance the loading.

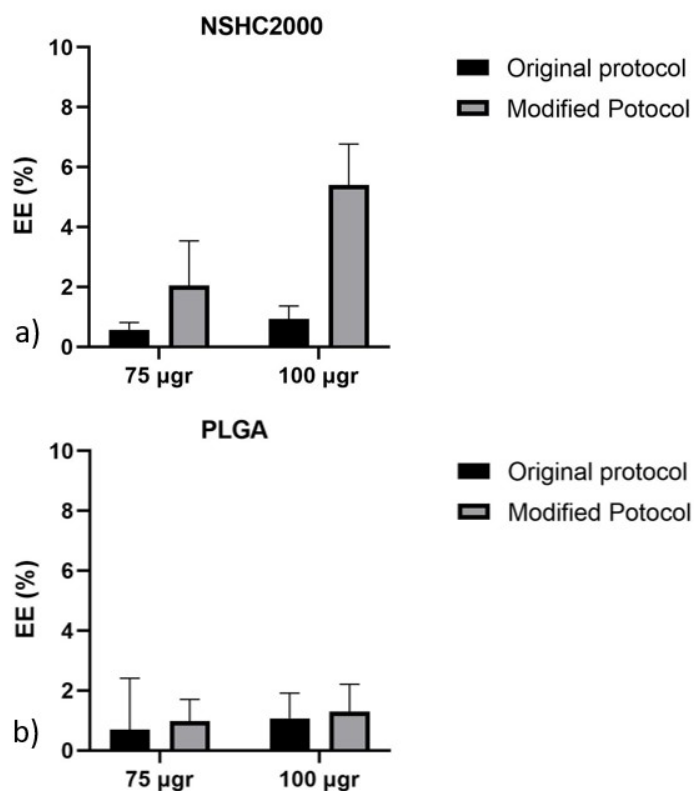


Figure 16: Drug Entrapment Efficacy comparison between original and modified protocol for both a) NSHC2000 and b) PLGA.

3.1.3 Drug Release Test

Release tests were performed on NSHC2000 loaded NPs with 100 μ gr drug loading. As shown in Figure 17, a burst release of 55% of the initial encapsulated drug was observed during the first 24h, while the entire amount was released within a 1 week in a controlled fashion.

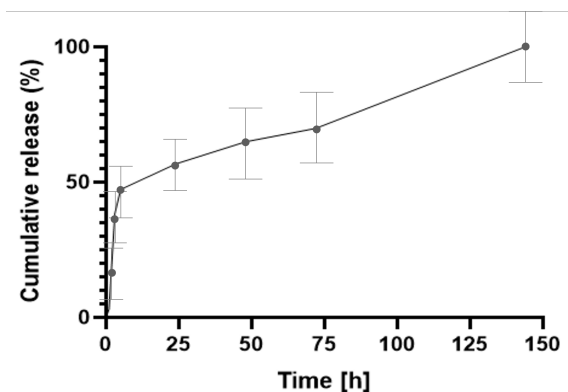


Figure 17: CCI-001 cumulative release in ddH₂O at 37°C over a week.

3.1.4 Yield

Process yield was calculated for NSHC2000 loaded NPs with 100 μ gr drug loading. The resulting yield was around \sim 66%, as shown in Figure 18.

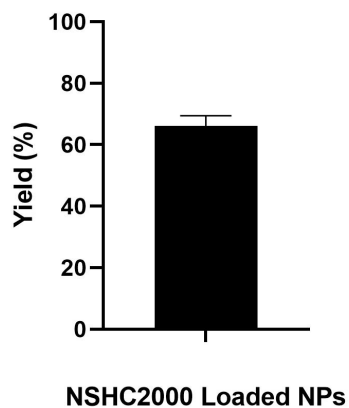


Figure 18: Process yield for NSHC2000 loaded NPs.

3.1.5 Stability in aqueous solution

Stability of the NPs suspension in water is reported in Figure 19. Slight fluctuations in size were observed, from 140 nm to 150 nm, albeit not significant. A decrease of zeta potential magnitude, from -37 mV to -22 mV was observed. These results may suggest a decrease in the suspension stability, however, steric protection of the particles (i.e. through pegylation, such as in this work), can prevent agglomeration at low ZP magnitudes [84].

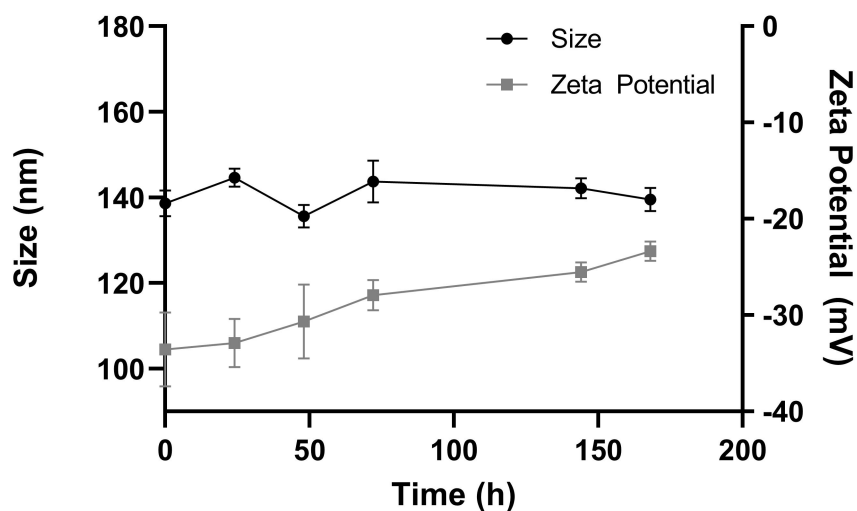


Figure 19: Size and Zeta Potential measurements over a week. NPs were stored in ddH₂O at 4°C.

3.1.6 Morphology

SEM imaging showed a marked aggregation of the NPs, as shown in Figure 20. This was probably due to the sample preparation conditions, that involves drying of the solution and subsequent sample metallization.

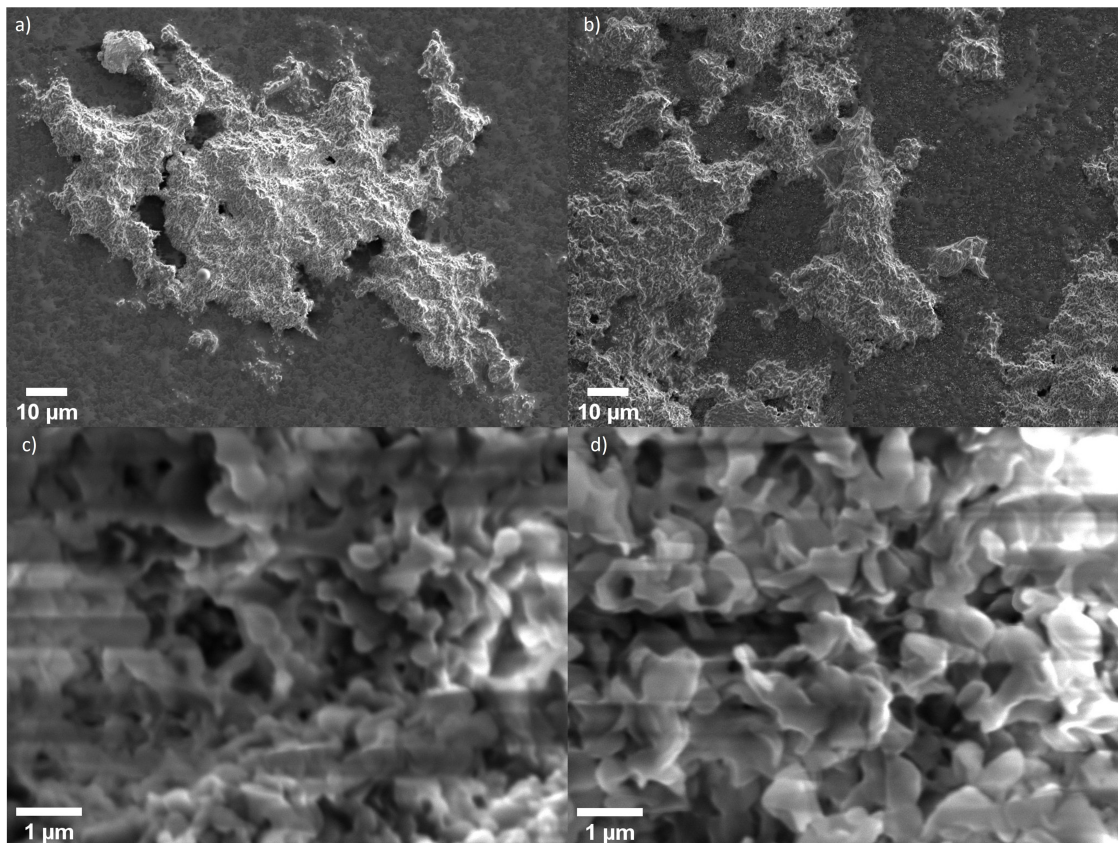


Figure 20: SEM images of blank a), c) and NSHC2000-loaded nanoparticles b),d), at different magnifications.

3.2 In vitro studies

3.2.1 Mia-PaCa-2 2D Culture

A comparison between MiaPaca-2 cells viabilities resulting from free CCI-001 and CCI-001-loaded NPs treatments at each time point is reported in Figure 21. Treatment with 1 nM concentration of CCI-001 was not effective at all, while CCI-001 efficacy was maximized at 72h, reaching 40% viability both for free CCI-001 and CCI-001-loaded NPs. For free CCI-001 treatment, no discernible differences in cells viability was seen for concentrations higher than 10 nM. For NPs treatment, CCI-001 started to show its effects at 20 nM concentrations and above. The higher viability in cells treated with NPs are to be attributed to the NPs delayed release of the drug. The two treatments showed the same overall efficacy, confirming the NPs suitability as drug carrier for CCI-001. MiaPaCa-2 cells can grow both as adherent and floating cells [87]. As shown in Figure 22, adherent cells detachment can be detected even at low concentrations both for free CCI-001 (5 nM) and for CCI-001-loaded NPs (10 nM) treatment.

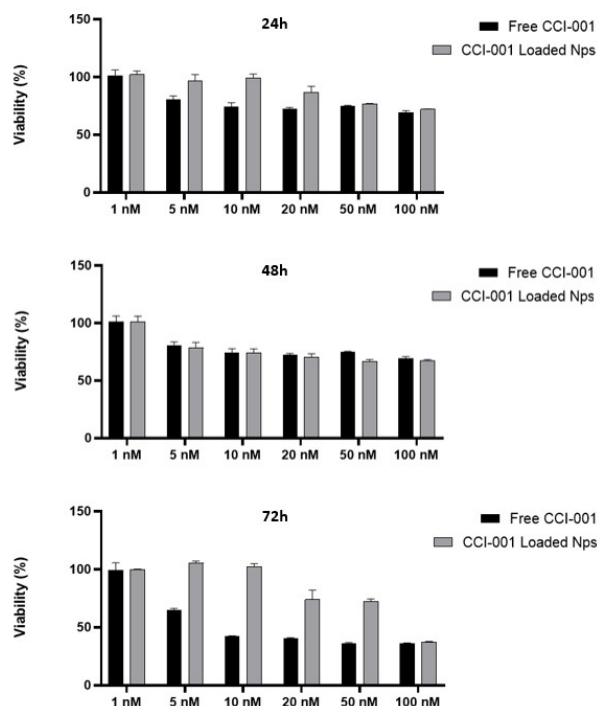


Figure 21: Comparison between MiaPaCa-2 cells viabilities resulting from treatments with free CCI-001 and CCI-001-loaded NPs at 1 nM, 5 nM, 10 nM, 20 nM, 50 nM and 100 nM at 24h, 48h, 72h.

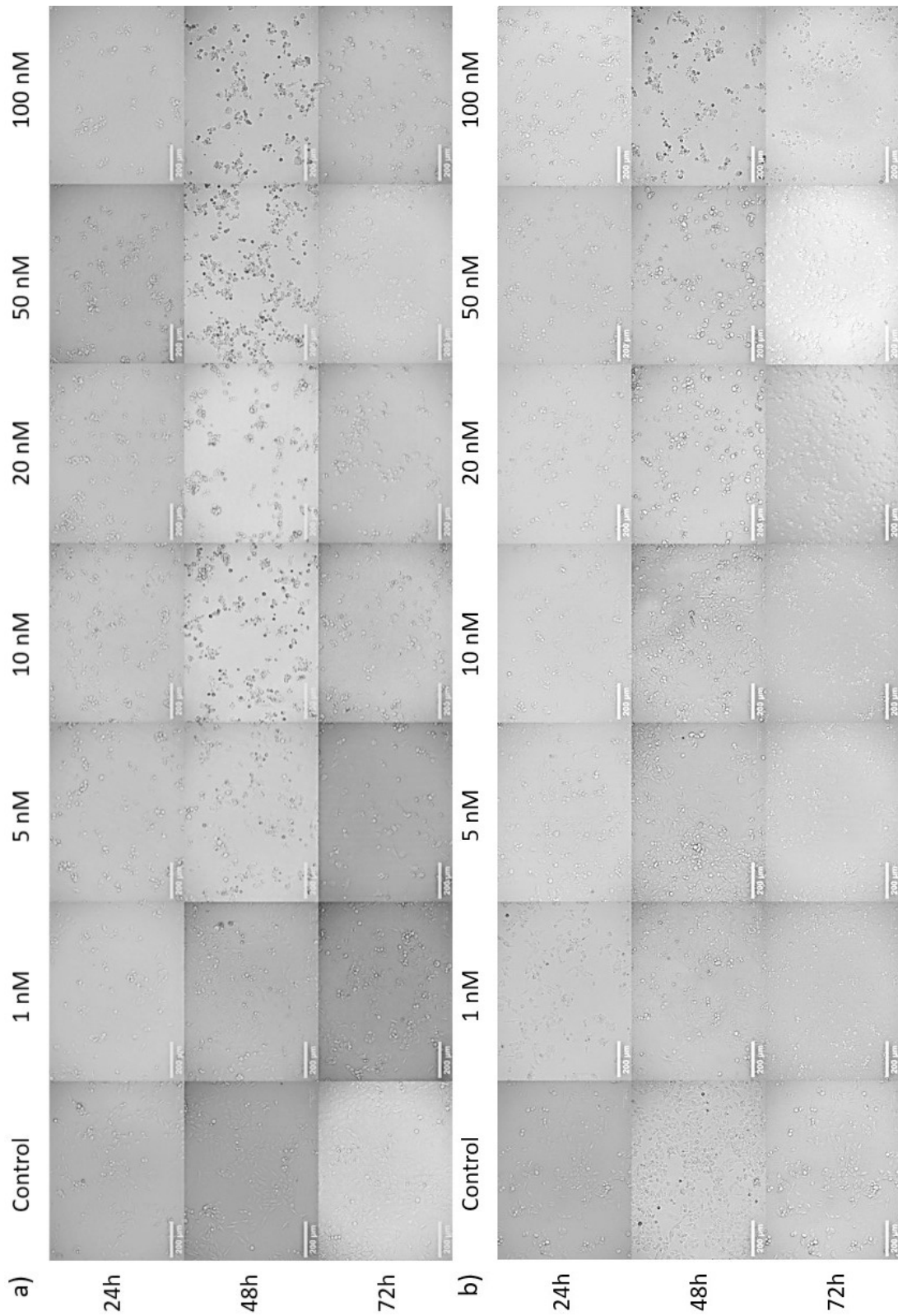


Figure 22: Cells images of MiaPaCa-2 cells treated with a) free CCI-001 and b) CCI-001-loaded NPs at 1 nM, 5 nM, 10 nM, 20 nM, 50 nM and 100 nM at 24h, 48h, 72h. Untreated cells are reported as control group. Scale bar=200 μm

3.2.2 U87MG 2D Culture

A comparison between U87MG cells viability after treatment with free CCI-001 and CCI-001-loaded NPs at each time point is reported in Figure 23. For free CCI-001, concentrations from 20 nM up to 100 nM were found effective against U87MG cells proliferation, reaching less than 15% cell viability for the highest concentration at 72h. CCI-001-loaded NPs treatments also showed concentration-dependent toxic effect, reaching 60% vital cells for the 100 nM treatment at 72h. As explained before, higher viabilities in cells treated with NPs are to be attributed to the NPs delayed release of the drug. The two treatments showed a comparable efficacy, confirming the NPs suitability as drug carrier for CCI-001. Cell images shown in Figure 24, demonstrate cell detachment at low concentrations both for free CCI-001 (1 nM) and for CCI-001-loaded NPs (5 nM), confirming their efficacy on this cell line.

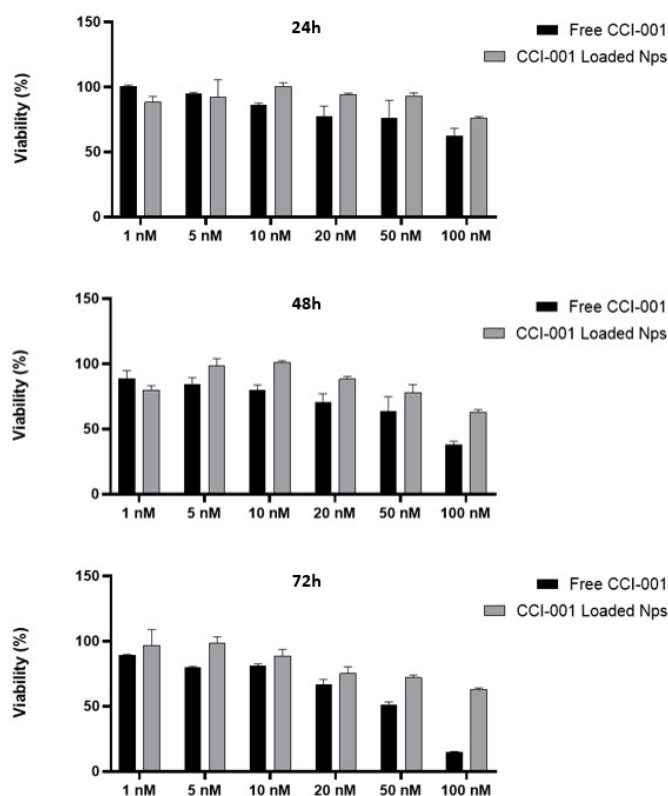


Figure 23: Comparison between U87MG cells viabilities resulting from treatments with free CCI-001 and CCI-001-loaded NPs at 1 nM, 5 nM, 10 nM, 20 nM, 50 nM and 100 nM at 24h, 48h, 72h.

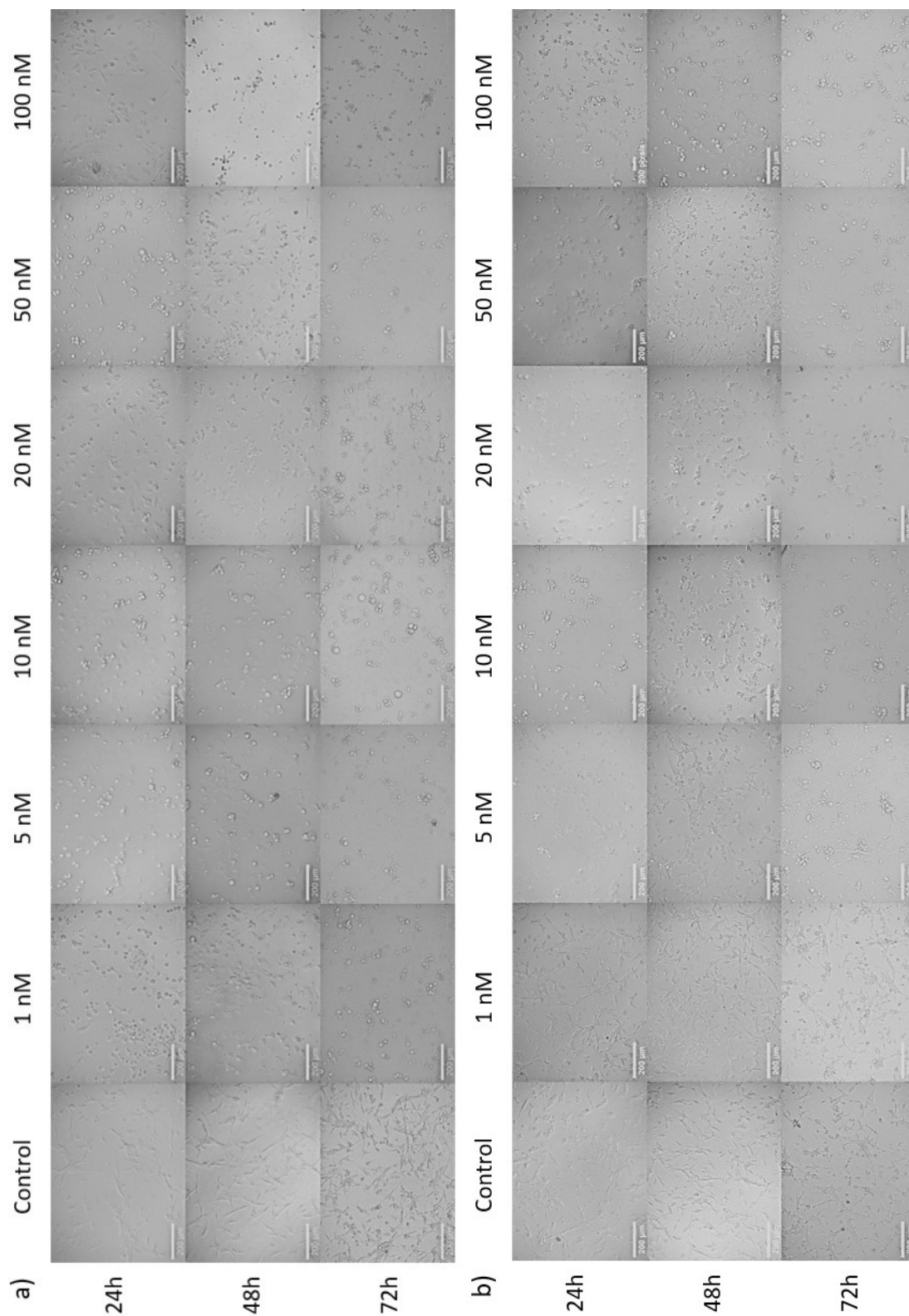


Figure 24: Cells images of U87MG cells treated with a) free CCI-001 and b) CCI-001-loaded NPs at 1 nM, 5 nM, 10 nM, 20 nM, 50 nM and 100 nM at 24h, 48h, 72h. Untreated cells are reported as control group. Scale bar=200 μm

3.2.3 Nanoparticles' U87MG cells internalization

Figure 25 shows poor internalization of Rhod-NPs inside U87MG GFP cells even at higher concentrations than those used for treatment with CCI-001. Internalization may be promoted by surface modifications of the NPs with targeted ligands.

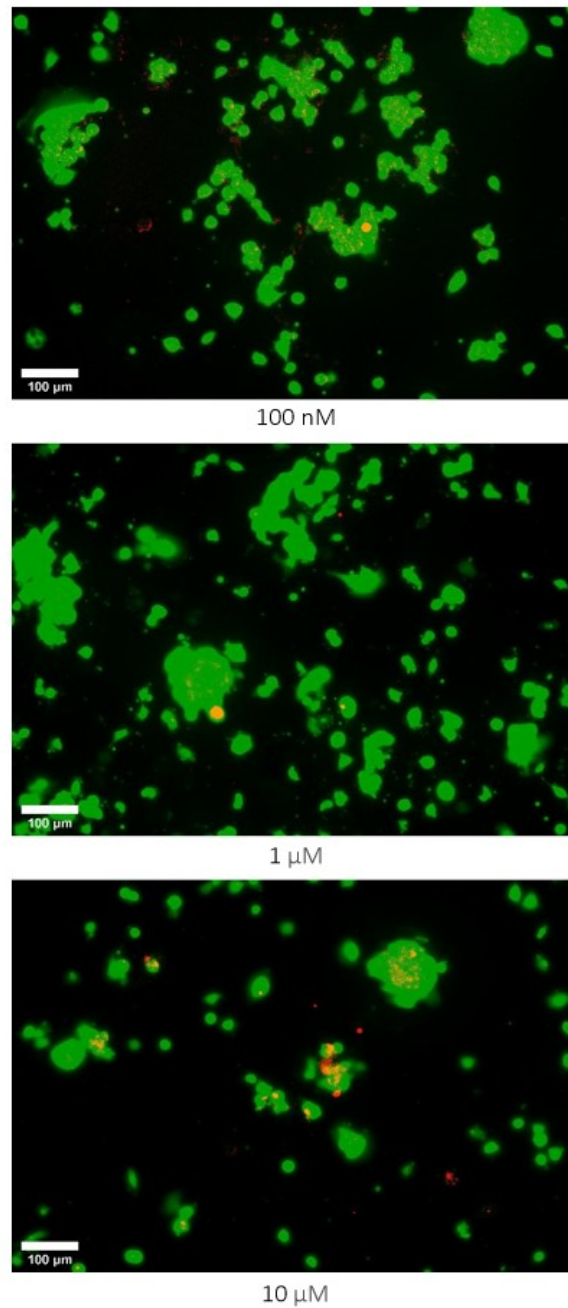


Figure 25: RGB images of U87MG GFP treated with Rhod-NPs at three concentrations (100nM, 1 μM and 10 μM) Scale bar=100 μm

3.2.4 U87MG Spheroids

A comparison between U87MG spheroids viability resulting from free CCI-001 and CCI-001-loaded NPs treatments at each time point is reported in Figure 26.

For free CCI-001 treatments, a decreasing trend in viabilities was observed starting from 48h of exposure to concentrations higher than 20 nM, reaching 40% viability for the 100 nM treatment at 72h. CCI-001-loaded NPs treatment showed the same trend, reaching less than 40% vital cells after 72h at the highest concentration. This difference may be explained by the better infiltration of NPs inside the spheroid compared to the free drug, improving CCI-001 transport. Spheroids images (Figure 27) show disgregation of the edges, which was more pronounced for the NPs treatments as compared to free drug treatments.

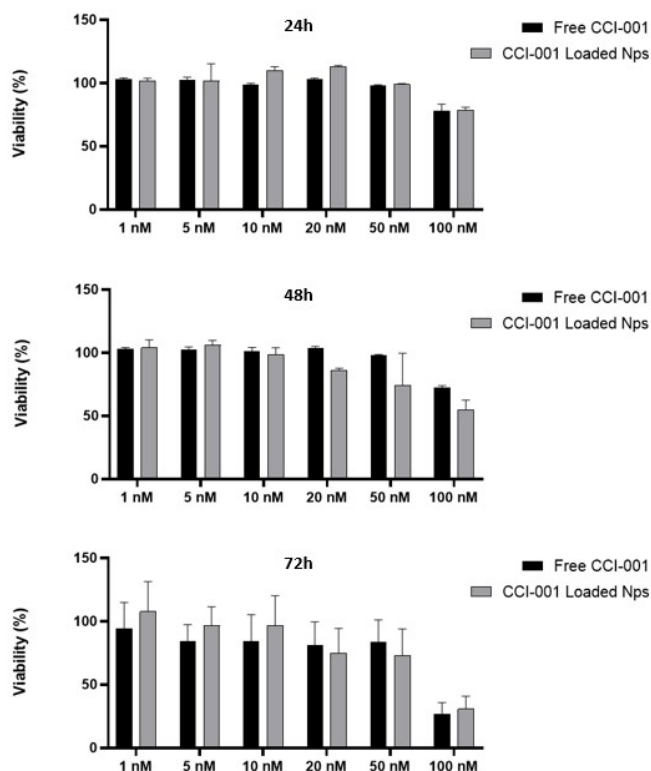


Figure 26: Comparison between U87MG spheroids viabilities resulting from treatments with free CCI-001 and CCI-001-loaded NPs at 1 nM, 5 nM, 10 nM, 20 nM, 50 nM and 100 nM at 24h, 48h, 72h.

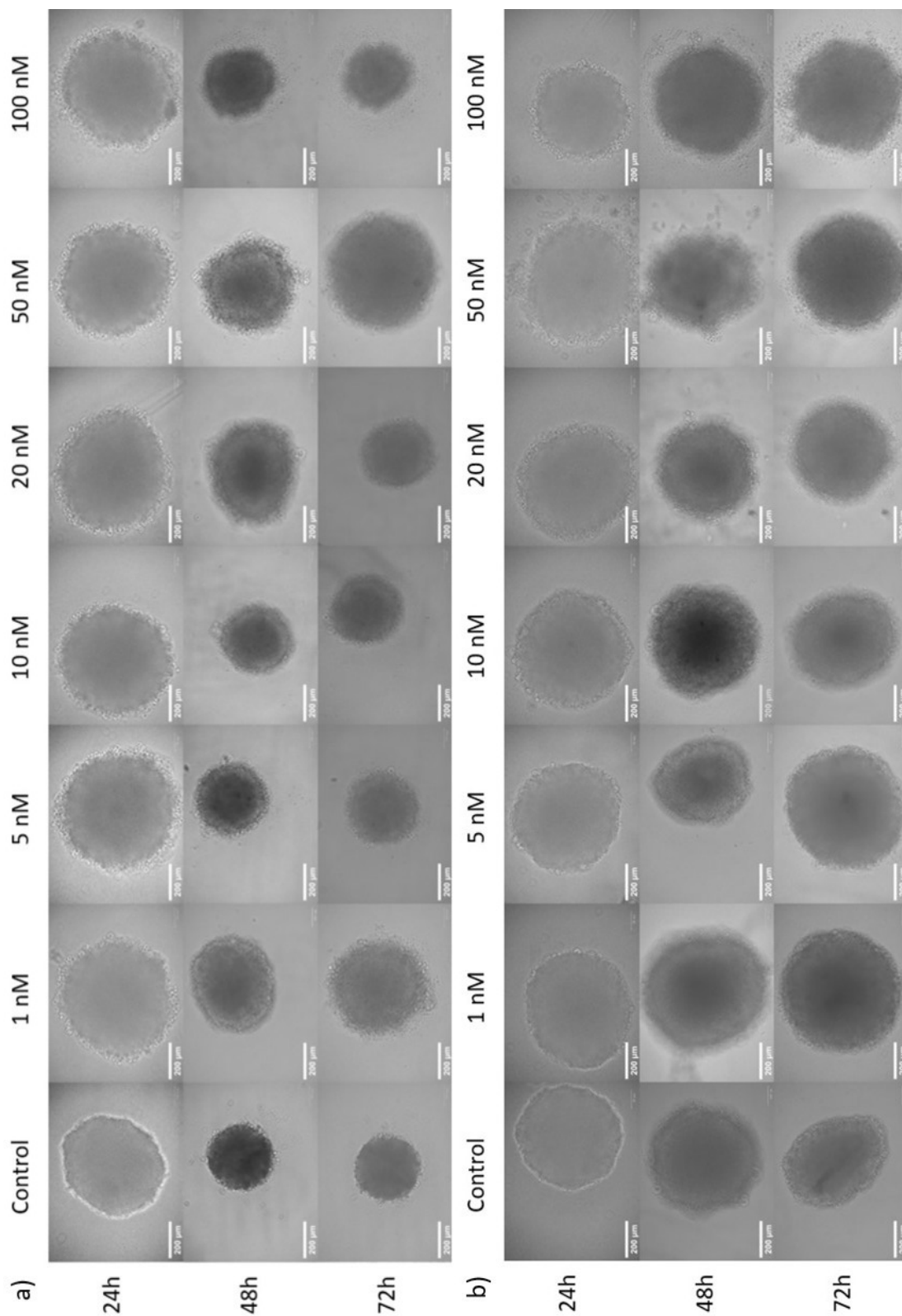


Figure 27: Cells images of MiaPaCa-2 cells treated with a) free CCI-001 and b) CCI-001-loaded NPs at 1 nM, 5 nM, 10 nM, 20 nM, 50 nM and 100 nM at 24h, 48h, 72h. Untreated cells are reported as control group. Scale bar=200 μm

3.2.5 Nanoparticles' U87MG spheroids infiltration

Figure 28 shows successful NPs infiltration inside the spheroids was observed for every NPs concentration at each time point, confirming the expected results.

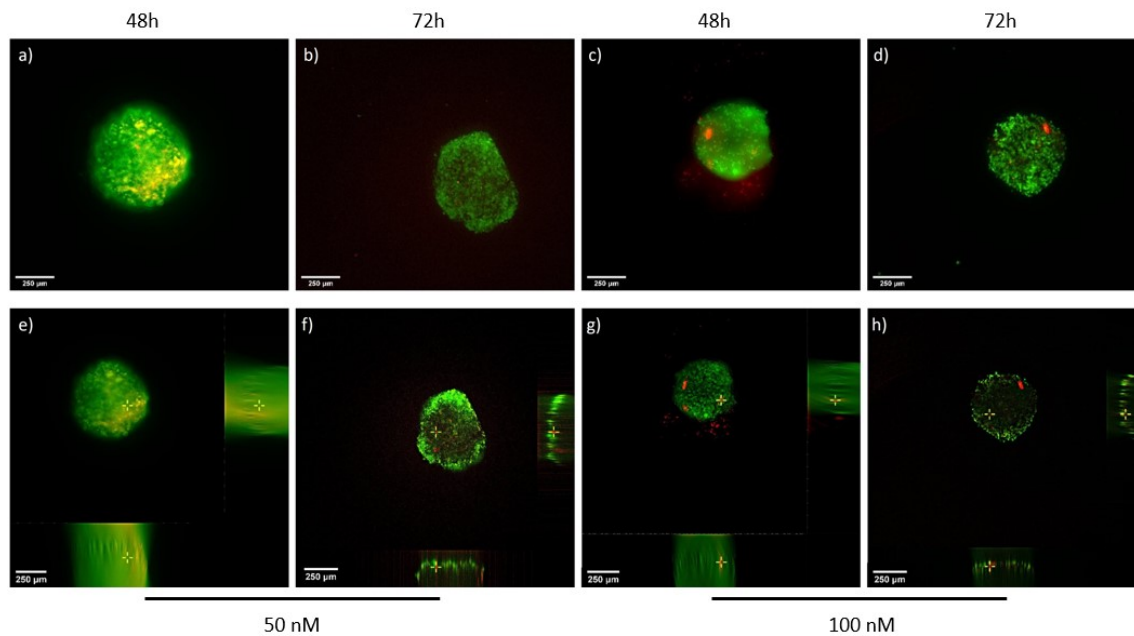


Figure 28: RGB images of U87MG GFP spheroids, treated with two Rhod-NPs concentrations (50 nM, 100 nM) and observed at 48h and 72h. a), b), c), and d) are superimposed images, e), f), g), h) show both frontal and lateral projections of the single slices for a given point, indicated by a yellow scope. Scale bar=250 μm

4 Conclusions

In this study we successfully developed self-assembled hybrid NPs with a core-shell structure that present small size, in the range of the EPR effect, and narrow size distribution. Also, negative zeta potential of this formulation is advantageous, as cells tend to internalize negatively charged NPs more easily. NPs stability was assessed, confirming that they can be stored in aqueous solution at 4°C for up to a week. Unfortunately, NPs morphology could not be studied using SEM microscopy, as the NPs were disrupted in the sample preparation process. Further studies on NPs morphology could be performed with TEM microscopy, which does not require samples' metallization. *In vitro* test demonstrated CCI-001 efficacy even at low concentrations (10 nM for MiaPaCa-2 cell line and 20 nM for U87MG cell line), confirming the results of previous studies. CCI-001-loaded NPs showed a similar efficacy to free CCI-001, as the higher viabilities in cells treated with NPs can be attributed to the delayed release, confirming that our nanoformulation is suitable for the delivery of this drug. *In vitro* tests on spheroids demonstrated even higher efficacy of CCI-001-loaded NPs compared to free CCI-001, probably due to enhanced drug transport, as NPs infiltration inside the spheroids can speed up the internalization process across the entire construct. Cells internalization and successful spheroids infiltration of NPs has been assessed only qualitatively, therefore quantitative studies (e.g. by FACS) are required in future studies. CCI-001-loaded NPs will be tested in future studies on the target tumors cell lines intended for CCI-001, such as OVCAR-3 cells, an ovarian cancer cell line. In addition, co-encapsulation of other drugs such as PROTAC could further improve treatment efficacy.

5 Acknowledgements

I would like to express all my gratitude to:

- My supervisors Prof. Gianluca Ciardelli, Prof. Jack Tuszynski and Prof. Clara Mattu for the opportunity they gave me to pursue this Master's thesis and their guidance throughout this project.
- Marialucia and Andrea, for their help and comprehension everytime I needed.
- My beloved parents and brother, who never made me miss anything, for having always believed in me and cheered me up with their love and affection.
- My girlfriend Miriam, for being constantly present for me despite the difficult times we both went through and for all the love you always showed me. For seven years you have been pushing me to be the best version of myself. I love you.
- All my colleagues who shared with me these five years of study, with whom I shared my first experience living away from my home city, they never made me feel away from Sicily. Also, the new colleagues I met during this master's degree.
- Last, but not least, my closest friends that always has been there for me, for all the laughs and tears we shared.

References

- [1] Jacques Ferlay, Isabelle Soerjomataram, Rajesh Dikshit, Sultan Eser, Colin Mathers, Marise Rebelo, Donald Maxwell Parkin, David Forman, and Freddie Bray. Cancer incidence and mortality worldwide: Sources, methods and major patterns in GLOBOCAN 2012. *International Journal of Cancer*, 136(5):E359–E386, 2015.
- [2] Elham Bidram, Yasaman Esmaeili, Hadi Ranji-Burachaloo, Nuha Al-Zaubai, Ali Zarrabi, Alastair Stewart, and Dave E. Dunstan. A concise review on cancer treatment methods and delivery systems. *Journal of Drug Delivery Science and Technology*, 54(July):101350, 2019.
- [3] Brandon Milholland, Xiao Dong, Lei Zhang, Xiaoxiao Hao, Yousin Suh, and Jan Vijg. Differences between germline and somatic mutation rates in humans and mice. *Nature Communications*, 8(May):1–8, 2017.
- [4] S Chakraborty and T Rahman. The difficulties in cancer treatment. pages 1–5, 2012.
- [5] Yousef Fouad and Carmen Aanei. Revisiting the hallmarks of cancer. *American journal of cancer research*, 7:1016–1036, 05 2017.
- [6] Roberta Lugano, Mohanraj Ramachandran, and Anna Dimberg. Tumor angiogenesis: causes, consequences, challenges and opportunities. *Cellular and Molecular Life Sciences*, 77(9):1745–1770, 2020.
- [7] Dietmar W. Siemann. The unique characteristics of tumor vasculature and preclinical evidence for its selective disruption by Tumor-Vascular Disrupting Agents. *Cancer Treatment Reviews*, 37(1):63–74, 2011.
- [8] Timothy P Padera, Ananth Kadambi, Emmanuelle Tomaso, Carla Mouta Carreira, Edward B Brown, Yves Boucher, Noah C Choi, Douglas Mathisen, John Wain, Eugene J Mark, Lance L Munn, Rakesh K Jain, Noah C Choi, Douglas Mathisen, John Wain, and Eugene J Mark. Lymphatic Metastasis in the Absence of Functional Intratumor Lymphatics Published by : American Association for the Advancement of Science Stable URL : <http://www.jstor.org/stable/3076953> REFERENCES Linked references are available on JSTOR for this articl. 296(5574):1883–1886, 2016.

- [9] Patricia Steeg. Tumor metastasis: Mechanistic insights and clinical challenges. *Nature medicine*, 12:895–904, 09 2006.
- [10] Lynda Wyld, Riccardo A. Audisio, and Graeme J. Poston. The evolution of cancer surgery and future perspectives. *Nature Reviews Clinical Oncology*, 12(2):115–124, 2015.
- [11] Helen H.W. Chen and Macus Tien Kuo. Improving radiotherapy in cancer treatment: Promises and challenges. *Oncotarget*, 8(37):62742–62758, 2017.
- [12] Bruce A. Chabner and Thomas G. Roberts. Chemotherapy and the war on cancer. *Nature Reviews Cancer*, 5(1):65–72, 2005.
- [13] Alex D. Waldman, Jill M. Fritz, and Michael J. Lenardo. A guide to cancer immunotherapy: from T cell basic science to clinical practice. *Nature Reviews Immunology*, 20(11):651–668, 2020.
- [14] Troy A Baudino. Send Orders for Reprints to reprints@benthamscience.ae Targeted Cancer Therapy: The Next Generation of Cancer Treatment. *Current Drug Discovery Technologies*, 12:3–20, 2015.
- [15] J Hematol, Zhe Cheng, Maoyu Li, Raja Dey, and Yongheng Chen. Nanomaterials for cancer therapy : current progress and perspectives. *Journal of Hematology Oncology*, pages 1–27, 2021.
- [16] Joydeb Majumder and Tamara Minko. Targeted Nanotherapeutics for Respiratory Diseases: Cancer, Fibrosis, and Coronavirus. *Advanced Therapeutics*, 4(2), 2021.
- [17] Yasuhiro Matsumura and Hiroshi Maeda. A New Concept for Macromolecular Therapeutics in Cancer Chemotherapy: Mechanism of Tumoritropic Accumulation of Proteins and the Antitumor Agent Smancs1. *Cancer Research*, 46(12_{part1}) : 6387 – –6392, 121986.
- [18] Jun Wu. The Enhanced Permeability and Retention (EPR) Effect : The Significance of the Concept and Methods to Enhance Its Application. 2021.
- [19] Rachel K O Reilly and Amanda K Pearce. Insights into active targeting of nanoparticles in drug delivery : advances in clinical studies and design considerations for cancer nanomedicine Insights into active targeting of nanoparticles in drug delivery : advances in clinical studies and design considerations for cancer. 2019.

- [20] Nicolas Bertrand, Jun Wu, Xiaoyang Xu, Nazila Kamaly, and Omid C Farokhzad. Cancer nanotechnology: The impact of passive and active targeting in the era of modern cancer biology. *Advanced Drug Delivery Reviews*, pages 1–24, 2013.
- [21] Aaron C. Anselmo and Samir Mitragotri. Nanoparticles in the clinic. *Bioengineering Translational Medicine*, 1(1):10–29, 2016.
- [22] Muhammad Raza Shah, Muhammad Imran, and Shafi Ullah. Chapter 2 - nanostructured lipid carriers. In Muhammad Raza Shah, Muhammad Imran, and Shafi Ullah, editors, *Lipid-Based Nanocarriers for Drug Delivery and Diagnosis*, Micro and Nano Technologies, pages 37–61. William Andrew Publishing, 2017.
- [23] Ron Hardman. A toxicologic review of quantum dots: Toxicity depends on physicochemical and environmental factors. *Environmental Health Perspectives*, 114(2):165–172, 2006.
- [24] Malik, Tanveer Bilal, Manoj Kumar, and Reiaz Rehman. *Biosynthesis of Nanoparticles and Their Application in Pharmaceutical Industry*, pages 331–349. 07 2017.
- [25] Arturo Sánchez, Susana P. Mejía, and Jahir Orozco. Recent advances in polymeric nanoparticle-encapsulated drugs against intracellular infections. *Molecules*, 25(16):1–45, 2020.
- [26] Parvin Ahmadiatabar, Amir A. Momtazi-Borojeni, Ali H. Rezayan, Mahboobeh Mahmoodi, Amirhossein Sahebkar, and Mostafa Mellat. Enhanced Entrapment and Improved in Vitro Controlled Release of N-Acetyl Cysteine in Hybrid PLGA/Lecithin Nanoparticles Prepared Using a Nanoprecipitation/Self-Assembly Method. *Journal of Cellular Biochemistry*, 118(12):4203–4209, 2017.
- [27] Sagar R Mudshinge, Amol B Deore, Sachin Patil, and Chetan M Bhalgat. Nanoparticles : Emerging carriers for drug delivery. *Saudi Pharmaceutical Journal*, 19(3):129–141, 2011.
- [28] Elvin Blanco, Haifa Shen, and Mauro Ferrari. Principles of nanoparticle design for overcoming biological barriers to drug delivery. *Nature Biotechnology*, 33(9):941–951, 2015.
- [29] Jung Soo Suk, Qingguo Xu, Namho Kim, Justin Hanes, and Laura M. Ensign. Pegylation as a strategy for improving nanoparticle-based drug and gene delivery. *Advanced Drug Delivery Reviews*, 99:28–51, 2016. Non-antigenic regulators of targeting for imaging and therapy.

- [30] A Hamilton, L Biganzoli, R Coleman, L Mauriac, P Hennebert, A Awada, M Nooij, L Beex, M Piccart, I Van Hoorebeeck, P Bruning, and D De Valeriola. Original article EORTC 10968 : a phase I clinical and pharmacokinetic study of polyethylene glycol liposomal doxorubicin (Caelyx $\text{\textcircled{R}}$, Doxil $\text{\textcircled{R}}$) at a 6-week interval in patients with metastatic breast cancer. pages 910–918, 2002.
- [31] J. Torin Huzil, Richard F. Ludueña, and Jack Tuszynski. Comparative modelling of human β tubulin isotypes and implications for drug binding. *Nanotechnology*, 17(4), 2006.
- [32] Caitlin M. Logan and A. Sue Menko. Microtubules: Evolving roles and critical cellular interactions. *Experimental Biology and Medicine*, 244(15):1240–1254, 2019.
- [33] Jun Zhou and Paraskevi Giannakakou. Targeting microtubules for cancer chemotherapy. *Current Medicinal Chemistry - Anti-Cancer Agents*, 5(1):65–71, 2005.
- [34] Antonina Roll-Mecak. The Tubulin Code in Microtubule Dynamics and Information Encoding. *Developmental Cell*, 54(1):7–20, 2020.
- [35] Amelia L. Parker, Maria Kavallaris, and Joshua A. McCarroll. Microtubules and their role in cellular stress in cancer. *Frontiers in Oncology*, 4 JUN(June):1–19, 2014.
- [36] Richard F. Ludueña. *A Hypothesis on the Origin and Evolution of Tubulin*, volume 302. Elsevier, 2013.
- [37] Arun Kanakkanthara and John H. Miller. β III-tubulin overexpression in cancer: Causes, consequences, and potential therapies. *Biochimica et Biophysica Acta - Reviews on Cancer*, 1876(2):188607, 2021.
- [38] Arun Kanakkanthara, Paul H Teesdale-spittle, and John H Miller. Cytoskeletal Alterations that Confer Resistance to Anti-tubulin Chemotherapeutics. pages 147–158, 2013.
- [39] Melissa C Pamula, Shih Chieh Ti, and Tarun M Kapoor. The structured core of human β tubulin confers isotype-specific polymerization properties. 213(4), 2016.
- [40] Kathy Kamath, Leslie Wilson, Fernando Cabral, and Mary Ann Jordan. III-Tubulin Induces Paclitaxel Resistance in Association with Reduced Effects on Microtubule Dynamic Instability *. *Journal of Biological Chemistry*, 280(13):12902–12907, 2005.

- [41] A Banerjee and R F Luduena. Kinetics of Colchicine Binding to Purified Tubulin Isootypes from Bovine Brain *. *Journal of Biological Chemistry*, 267(19):13335–13339, 1992.
- [42] C Stengel, S P Newman, M P Leese, B V L Potter, M J Reed, and A Purohit. Class III β -tubulin expression and in vitro resistance to microtubule targeting agents. *British Journal of Cancer*, pages 316–324, 2010.
- [43] Bing Cheng and Karen Crasta. Consequences of mitotic slippage for antimicrotubule drug therapy. 2017.
- [44] Joshua A Mccarroll, Pei Pei Gan, Marjorie Liu, and Maria Kavallaris. β III-Tubulin Is a Multifunctional Protein Involved in Drug Sensitivity and Tumorigenesis in Non – Small Cell Lung Cancer. pages 4995–5003.
- [45] Luis J Leandro-garcı, Marta Mendiola, Susanna Leskela, Beatriz Martı, Jorge Barriuso, Javier De Santiago, Mercedes Robledo, David Hardisson, and Cristina Rodrı. The miR-200 family controls β -tubulin III expression and is associated with paclitaxel-based treatment response and progression-free survival in ovarian cancer patients. pages 85–95, 2011.
- [46] Disruption Angiogenesis. Current Advances of Tubulin Inhibitors in Nanoparticle Drug Delivery and Vascular. 2016.
- [47] Qinghui Wang, Kinsie Arnst, Yuxi Wang, Gyanendra K Kumar, Dejian Ma, Stephen W White, Duane D Miller, Weimin Li, and Wei Li. Structure guided design , synthesis , and biological evaluation of analogs targeting the colchicine binding site in tubulin. 2019.
- [48] Jiani Wang, Michelle Cheng, Ivy K M Law, Christina Ortiz, Mingjun Sun, and Hon Wai Koon. Cathelicidin Suppresses Colon Cancer Metastasis via a P2RX7-Dependent Mechanism. *Molecular Therapy: Oncolytics*, 12(March):195–203, 2019.
- [49] Taxane-site Ligands, Francisco De As, Tobias Mühlethaler, Juan Est, Enrique Calvo, Juan Francisco, April L Risinger, Erik J Sorensen, Christopher D Vanderwal, Karlheinz Altmann, Susan L Mooberry, Michel O Steinmetz, Andrea E Prota, and J D Fernando. Crystal Structure of the Cyclostreptin-Tubulin Adduct : Implications for Tubulin Activation by. pages 1–17, 2019.

- [50] Vladimír Čermák, Vojtěch Dostál, Michael Jelínek, Lenka Libusová, Jan Kovář, Daniel Rösel, and Jan Brábek. Microtubule-targeting agents and their impact on cancer treatment. *European Journal of Cell Biology*, 99(4), 2020.
- [51] Linda Wordeman and Juan Jesus Vicente. Microtubule targeting agents in disease: Classic drugs, novel roles. *Cancers*, 13(22), 2021.
- [52] Eva Nogales, Sharon G. Wolf, and Kenneth H. Downing. Structure of the $\alpha\beta$ tubulin dimer by electron crystallography. *Nature*, 391(6663):199–203, 1998.
- [53] Irving S. Johnson, James G. Armstrong, Marvin Gorman, and J. Paul Burnett. The Vinca Alkaloids: A New Class of Oncolytic Agents. *Cancer Research*, 23(77):1390–1427, 1963.
- [54] Lorenzo Pallante, Antonio Rocca, Greta Klejborowska, Adam Huczynski, Gianvito Grasso, Jack A. Tuszynski, and Marco A. Deriu. In silico Investigations of the Mode of Action of Novel Colchicine Derivatives Targeting β -Tubulin Isotypes: A Search for a Selective and Specific β -III Tubulin Ligand. *Frontiers in Chemistry*, 8(February), 2020.
- [55] Frederika Mandelbaum-Shavit, Mary K. Wolpert-DeFilippes, and David G. Johns. Binding of maytansine to rat brain tubulin. *Biochemical and Biophysical Research Communications*, 72(1):40–46, 1976.
- [56] Kylie A. Hood, Lyndon M. West, Berber Rouwé, Peter T. Northcote, Michael V. Berridge, St John Wakefield, and John H. Miller. Peloruside A, a novel antimetabolic agent with paclitaxel-like microtubule-stabilizing activity. *Cancer Research*, 62(12):3356–3360, 2002.
- [57] Shinichi Kobayashi, Kouichi Tsuchiya, Mituyuki Nishide, Takaaki Nishikiori, Taizo Nakagawa, and Nobuyoshi Shimada. Pironetin, a Novel Plant Growth Regulator Produced by *Streptomyces* sp. NK10958 III. Biosynthesis. *Journal of Antibiotics*, 48(8):893–895, 1995.
- [58] Susan Matthew, Qi Yin Chen, Ranjala Ratnayake, Charles S. Fermaintt, Daniel Lucena-Agell, Francesca Bonato, Andrea E. Prota, Seok Ting Lim, Xiaomeng Wang, J. Fernando Díaz, April L. Risinger, Valerie J. Paul, Maria Ángela Oliva, and Hendrik Luesch. Gatorbulin-1, a distinct cyclodepsipeptide chemotype, targets a seventh tubulin pharmacological site. *Proceedings of the National Academy of Sciences of the United States of America*, 118(9):1–11, 2021.

- [59] Yaron Finkelstein, Steven E. Aks, Janine R. Hutson, David N. Juurlink, Patricia Nguyen, Gal Dubnov-Raz, Uri Pollak, Gideon Koren, and Yedidia Bentur. Colchicine poisoning: The dark side of an ancient drug. *Clinical Toxicology*, 48(5):407–414, 2010.
- [60] Tae Jin Kim, Murali Ravoori, Charles N Landen, Aparna A Kamat, Liz Y Han, Chunhua Lu, Yvonne G Lin, William M Merritt, Nicholas Jennings, Whitney A Spannuth, Robert Langley, David M Gershenson, Robert L Coleman, Vikas Kundra, and Anil K Sood. Antitumor and Antivascular Effects of AVE8062 in Ovarian Carcinoma. (19):9337–9345, 2007.
- [61] Edward B Garon, Jeffrey D Neidhart, and Nashat Y Gabrail. A randomized Phase II trial of the tumor vascular disrupting agent CA4P (fosbretabulin tromethamine) with carboplatin , paclitaxel , and bevacizumab in advanced nonsquamous non-small-cell lung cancer. pages 7275–7283, 2016.
- [62] Edward L. Schwartz. Antivascular actions of microtubule-binding drugs. *Clinical Cancer Research*, 15(8):2594–2601, 2009.
- [63] Guido Koch. Medicinal Chemistry. *Chimia*, 71(10):643, 2017.
- [64] Cheol Hee Choi. ABC transporters as multidrug resistance mechanisms and the development of chemosensitizers for their reversal. *Cancer Cell International*, 5:1–13, 2005.
- [65] Md Lutful Amin. P-glycoprotein inhibition for optimal drug delivery. *Drug Target Insights*, 2013(7):27–34, 2013.
- [66] Ying Ying Leung, Laura Li, Yao Hui, and Virginia B Kraus. Author ’ s Accepted Manuscript. *Seminars in Arthritis and Rheumatism*, 2015.
- [67] Zeinab Saleh and Thurayya Arayssi. Update on the therapy of Behçet disease. *Therapeutic Advances in Chronic Disease*, 5(3):112–134, 2014.
- [68] Kristen Bova Campbell, Teresa A. Cicci, Alyssa K. Vora, and Lindsey D. Burgess. Beyond gout: Colchicine use in the cardiovascular patient. *Hospital Pharmacy*, 50(10):859–867, 2015.
- [69] Tao Zhang, Wei Chen, Xumian Jiang, Lei Liu, Kai Wei, Hansong Du, Hui Wang, and Juan Li. Anticancer effects and underlying mechanism of Colchicine on human gastric cancer cell lines in vitro and in vivo. *Bioscience Reports*, 39(1):1–10, 2019.

- [70] Ashok Kumar, Parduman R. Sharma, and Dilip M. Mondhe. Potential anticancer role of colchicine-based derivatives: An overview. *Anti-Cancer Drugs*, 28(3):250–262, 2016.
- [71] Jung Hae Cho, Young Hoon Joo, Eun Young Shin, Eun Ji Park, and Min Sik Kim. Anticancer effects of colchicine on hypopharyngeal cancer. *Anticancer Research*, 37(11):6269–6280, 2017.
- [72] Patrick A Curmi, Marcel Knossow, Isabelle Jourdain, and Sylvie Lachkar. Insight into tubulin regulation from a complex with colchicine and a stathmin-like domain. 428(MARCH):198–202, 2004.
- [73] H. William Detrich, Robley C. Williams, and Leslie Wilson. Effect of Colchicine Binding on the Reversible Dissociation of the Tubulin Dimer. *Biochemistry*, 21(10):2392–2400, 1982.
- [74] Jing Chen, Tao Liu, Xiaowu Dong, and Yongzhou Hu. Recent Development and SAR Analysis of Colchicine Binding Site Inhibitors. pages 1174–1190, 2009.
- [75] E A Woltering. Colchicine and 2-methoxyestradiol Inhibit Human Angiogenesis. 108:104–108, 2005.
- [76] Ibrahim M. Abdulbaqi, Yusrida Darwis, Reem Abou Assi, and Nurzalina Abdul Karim Khan. Transethosomal gels as carriers for the transdermal delivery of colchicine: Statistical optimization, characterization, and ex vivo evaluation. *Drug Design, Development and Therapy*, 12:795–813, 2018.
- [77] O Queirós, F Baltazar, S U, and A Goffeau. The anticancer agent 3-bromopyruvate : a simple but powerful molecule taken from the lab to the bedside. pages 349–362, 2016.
- [78] Alessandra Spada, Jaber Emami, Forough Sanaee, Maral Aminpour, Igor M. Paiva, Jack A. Tuszynski, and Afsaneh Lavasanifar. Albumin nanoparticles for the delivery of a novel inhibitor of β -tubulin polymerization. *Journal of Pharmacy and Pharmaceutical Sciences*, 24(5):344–362, 2021.
- [79] C. E. Mora-Huertas, H. Fessi, and A. Elaissari. Influence of process and formulation parameters on the formation of submicron particles by solvent displacement and emulsification-diffusion methods: Critical comparison. *Advances in Colloid and Interface Science*, 163(2):90–122, 2011.

- [80] Yun Liu, Guangze Yang, Thejus Baby, Tengjisi, Dong Chen, David A. Weitz, and Chun Xia Zhao. Stable Polymer Nanoparticles with Exceptionally High Drug Loading by Sequential Nanoprecipitation. *Angewandte Chemie - International Edition*, 59(12):4720–4728, 2020.
- [81] H. Fessi, F. Puisieux, J. Ph Devissaguet, N. Ammoury, and S. Benita. Nanocapsule formation by interfacial polymer deposition following solvent displacement. *International Journal of Pharmaceutics*, 55(1):1–4, 1989.
- [82] Moses Isabirye, D.V.N Raju, M. Kitutu, V. Yemeline, J. Deckers, and J. Poesen Additional. We are IntechOpen , the world ' s leading publisher of Open Access books Built by scientists , for scientists TOP 1 *Intech*, page 13, 2012.
- [83] M. Danaei, M. Dehghankhold, S. Ataei, F. Hasanzadeh Davarani, R. Javanmard, A. Dokhani, S. Khorasani, and M. R. Mozafari. Impact of particle size and polydispersity index on the clinical applications of lipidic nanocarrier systems. *Pharmaceutics*, 10(2):1–17, 2018.
- [84] Soheyla Honary and Foruhe Zahir. Effect of zeta potential on the properties of nano-drug delivery systems - A review (Part 1). *Tropical Journal of Pharmaceutical Research*, 12(2):255–264, 2013.
- [85] Promega Corporation. CellTiter 96 [®] AQueous One Solution Cell Proliferation Assay. *Www.Promega.Com/Protocols/*, pages 2014–12–15, 2012.
- [86] Shahed Behzadi, Vahid Serpooshan, Wei Tao, Majd A. Hamaly, Mahmoud Y. Alkawareek, Erik C. Dreaden, Dennis Brown, Alaaldin M. Alkilany, Omid C. Farokhzad, and Morteza Mahmoudi. Cellular uptake of nanoparticles: Journey inside the cell. *Chemical Society Reviews*, 46(14):4218–4244, 2017.
- [87] Norihiko Sasaki, Fujiya Gomi, Fumio Hasegawa, Kazumi Hirano, Masakazu Fujiwara, Masashi Toyoda, and Toshiyuki Ishiwata. Characterization of the metastatic potential of the floating cell component of MIA PaCa-2, a human pancreatic cancer cell line. *Biochemical and Biophysical Research Communications*, 522(4):881–888, 2020.